

The nature of intermediate-redshift damped Ly α absorbers^{*}

V. Le Brun¹, J. Bergeron^{2,3}, P. Boissé⁴, and J.M. Deharveng¹

¹ Laboratoire d'Astronomie Spatiale du C.N.R.S., B.P. 8, F-13376 Marseille CEDEX 12, France, vlebrun@astrsp-mrs.fr, jmd@astrsp-mrs.fr

² European Southern Observatory, Karl-Schwarzschild-Straße 2., D-85748 Garching b. München, Germany, jbergero@eso.org

³ Institut d'Astrophysique de Paris, CNRS, 98bis boulevard Arago, F-75014 Paris, France

⁴ Ecole Normale Supérieure, 24 rue Lhomond, F-75005 Paris, France, boisse@ensapa.ens.fr

Received May 24th, 1996; accepted Oct 24th, 1996

Abstract. We present HST/WFPC2 high-spatial resolution images in the R and B bands of the close environment of the sightlines to seven quasars which spectra show either a damped Ly α absorption line, 21 cm absorption, or a very strong Mg II/Fe II absorption system at intermediate redshifts ($0.4 \leq z \leq 1$). Objects down to about $0.3''$, or 2.0 kpc at $z = 0.6$ ($H_0 = 50 \text{ km s}^{-1} \text{ Mpc}^{-1}$, $q_0 = 0$), and to a limiting magnitude $m_{702, \text{lim}} = 25.9$ could be detected for seven fields comprising eight absorbers (one at higher redshift $z = 1.78$ towards MC 1331+170) with high H I column densities of at least $1 \times 10^{20} \text{ cm}^{-2}$.

In each case, a candidate absorber with absolute magnitude $M_B \simeq -19.0$ or much brighter has been detected. This small sample of gas-rich galaxies at intermediate redshifts covers a wide range in morphological types. There are three spiral galaxies of various sizes and luminosities (towards 3C 196, Q 1209+107 and MC 1331+170), three compact objects (towards EX 0302–223, PKS 0454+039 and, at high redshift, MC 1331+170), and two amorphous, low surface brightness galaxies (towards PKS 1229–021 and 3C 286). In the fields around 3C 196, PKS 1229–021 and Q 1209+107, there is an excess of galaxies in the PC2 images, suggestive of the presence of a group of galaxies associated with the damped Ly α absorber, or maybe with the quasar itself for the two $z_e \leq 1.0$ cases. For 3C 196 and 3C 286, the quasar host galaxies have also tentatively been discovered. We do not detect any quasar multiple images, implying no large amount of dark matter around the damped Ly α absorbers.

This survey also led to the discovery of the first $z \simeq 1.0$ optical counterpart of a quasar radio jet (PKS 1229–021).

Send offprint requests to: V. Le Brun

^{*} Based on observations made with the NASA/ESA *Hubble Space Telescope*, obtained at the Space Telescope Science Institute, which is operated by the Association of Universities for Research in Astronomy, Inc., under NASA contract NAS 5-26555

As will be reported elsewhere (Boissé et al. 1996), spectroscopy with the HST-FOS of the strong Mg II/Fe II absorption systems confirms the validity of our selection criterion in predicting the existence of damped Ly α systems.

Key words: quasar: absorption lines – galaxies: ISM – galaxies: halos

1. Introduction

Metal-rich absorption line systems (C IV and Mg II, damped Ly α and 21 cm systems) are a very powerful tool for studying the statistical properties of high-redshift young galaxies, otherwise very difficult to detect directly, but it must be ascertained which kind of population does indeed probe each type of system. The large column density absorbers giving rise to high-redshift damped Ly α absorption lines in quasar spectra are generally assumed to trace proto-galactic disks (Wolfe et al. 1986), whereas Mg II absorptions at intermediate redshifts trace the gaseous halos of luminous field galaxies (Bergeron & Boissé 1991, thereafter BB91; Steidel 1993) with typically radii of the order of $75h_{50}^{-1} \text{ kpc}$ (where h_{50} is the Hubble constant in units of $50 \text{ km s}^{-1} \text{ Mpc}^{-1}$, and using $q_0 = 0$). The main arguments that have led to associate the damped Ly α systems (DLAS) with the progenitors of present-day gas-rich galaxies are related to their mass density (Wolfe 1987) and to their metal content (Pettini et al. 1994). Nevertheless, the population producing the damped Ly α absorption lines is not yet unambiguously identified since the systems detected in the optical range are at too high redshifts ($z_d \geq 2$) to easily detect the absorber by its emission, both because of its apparent faintness and its proximity to the quasar image.

The aim of this project is to determine the magnitude, morphology, color and extent of the H I component

of the galaxies causing 21 cm/damped Ly α absorption at intermediate redshift and investigate whether these absorptions probe galactic disks, gaseous halos or elongated whip-like structures as in NGC 3067/3C 232 (Carilli & Van Gorkom 1989). This program is a first step towards relating the properties of present-day and intermediate-redshift gas-rich galaxies. When the project was undertaken, only a few 21 cm absorbers at intermediate redshift were known and no damped Ly α system had yet been discovered at $0.2 \leq z \leq 1.0$ from ultraviolet observations. As photoionization modeling had shown that Mg II systems with very strong Fe II associated absorption should have H I column densities in excess of a few 10^{19} cm^{-2} (Bergeron & Stasińska 1986), which is indeed the case for 21 cm absorbers, we also selected absorption systems displaying this property.

High spatial resolution images of the selected quasar fields were taken with the HST-Wide Field and Planetary Camera 2 (WFPC2), and UV spectroscopy was obtained with the HST-FOS to derive the H I column densities, the gas temperature for the 21 cm absorbers, and to set constraints on the heavy element abundances. The selected quasars exhibit at least one of the following properties:

- a 21 cm absorption: 3C 196, PKS 1229–021 and 3C 286,
- a high rest-frame equivalent width ratio $w_r(\text{Fe II})/w_r(\text{Mg II}) \sim 1$: EX 0302–223, Q 1209+107, PKS 0454+039, MC 1331+170,
- a damped Ly α line at higher redshift: MC 1331+170,
- a galaxy very close to the quasar sightline: PKS 1229–021 (Bergeron, unpublished CFHT observations), Q 1209+107 (Arnaud et al. 1988), 3C 196 (Boissé & Boulade 1990).

Four of these quasar fields have been previously studied with either the HST Wide Field Camera 2 (3C 196: Cohen et al. 1996) or ground-based telescopes (PKS 1229–021 and 3C 286: Steidel et al. 1994a, PKS 0454+039: Steidel et al. 1995). In each case, a candidate absorber was detected and these results will be discussed and compared to our higher spatial-resolution observations in Sect. 3.

In this paper we present the results obtained with the Planetary Camera 2 (PC2) for seven fields, seven damped Ly α candidate absorbers and one confirmed damped Ly α system. The observations, the method developed for the quasar image subtraction, and the algorithm used for the object detection, classification and magnitude estimate are described in Sect. 2. The individual fields are presented in Sect. 3. The implications of these observations are discussed in Sect. 4. The analysis of our spectroscopic data will be presented in Boissé et al. (1996) and the Wide Field Camera 2 (WFC2) observations will be discussed in a subsequent paper.

2. Observations and data reduction

2.1. Presentation of the observations

All the data were obtained with the Wide Field Planetary Camera 2 (WFPC2), using the filters F702W and F450W, with central wavelengths 6900 Å and 4550 Å respectively, except for MC 1331+170. For the latter, the damped Ly α absorber is at higher redshift, and we used the filters F702W and F814W (central wavelength 8300 Å). The Journal of the observations is given in Table 1. The zero-points of the magnitude scales are not those adopted in the HST-STMAG system. They were taken from Whitmore (1995) and Holtzman et al. (1995), since the zero-points of the STMAG system are based on a flat spectrum, whereas usual visible ground-based photometry is based on the Vega spectrum. Adopting a Vega-type spectrum to define the magnitude zero-points implies to add +0.487, –0.760 and –1.266 magnitudes to those of the STMAG for the F450W, F702W and F814W filters respectively.

To compare the HST photometric magnitudes to those obtained for ground-based observations and to derive the differential magnitude number counts, we have used the color equation given by Holtzmann et al. (1995) for the transformation from HST to *UBVRI* magnitude systems together with the mean values $B - V = 0.7$ and $V - R = 0.7$, corresponding to an intermediate galaxy type at $z \leq 1$ (Frei & Gunn 1994). The derived average color terms are $B - m_{450} = 0.15$ and $R - m_{702} = 0.35$. For the F814W data, no correction is needed to recover the *I* magnitude, the correction-term being very small.

Each quasar was located at the center of the PC2 field. The PC2 pixel size is $0.046''$, its field of view is $36'' \times 36''$ wide, and the spatial resolution is $\text{FWHM} = 0.103''$, $0.123''$ in the *x* and *y* directions respectively for the raw data, and $\text{FWHM} = 0.129''$, $0.143''$ after the $\sigma = 0.5$ pixel Gaussian smoothing that we used for the presentation of the data. These values are measured on the non-saturated star of the field of Q 1209+107 (object #3, see Fig. 8), and are consistent with those given in the WFPC2 handbook. For each target, several exposures were obtained (at least four for the F702W images), to allow a better rejection of the cosmic rays events and to minimize saturation of the quasar. In fact, the number of cosmic rays is important (about 1300 per PC2 field for a 900 s exposure), and more than three exposures are necessary to properly remove them. The hot and corrupted pixels, which appear on all the exposures, have been removed using the chart provided by the STScI. The remaining hot pixels are removed using an adapted median filter.

2.2. Detection of the objects and photometry

The detection and classification of the objects present in the PC2 fields were made using the software Source Extractor package (Bertin & Arnouts 1996), which offers very robust object detection, high quality deblending, and good

Table 1. Journal of the observations

Object	Coordinates (J2000)		z_e	z_a^a (metal-rich systems)	Date	Filter	$n \times \Delta t$	m_{lim}
	R.A.	Dec						
EX 0302–223	03 04 50.1	–22 11 57	1.400	1.0095 (DLAS cand.) 0.4196 (Mg II)	1994, Jun 4	F450W	4×500	25.27
PKS 0454+039	04 56 47.1	+04 00 53	1.345	0.8596 (DLAS) 0.072 (Mg II) 1.0680 (C IV) 1.1536 (Mg II/C IV)	1994, Apr 7	F450W F702W	4×500 6×600	25.25 25.75
3C 196	08 13 36.0	+48 13 03	0.871	0.437 (DLAS, 21 cm) 0.871 (Mg II)	1994, Apr 16 1995, Apr 16	F450W F702W	2×1000 4×900	25.52 25.97
Q 1209+107	12 11 40.6	+10 30 03	2.191	0.6295 (DLAS cand.) 0.3930 (Mg II) 1.8434 (Mg II)	1994, Nov 11	F450W F702W	2×1000 4×900	25.65 25.86
PKS 1229–021	12 32 00.0	–02 24 05	1.038	0.39498 (DLAS, 21 cm) 0.7005 (C IV) 0.7568 (Mg II)	1994, May 18 1995, May 18	F450W F702W	4×500 6×600	25.22 25.83
3C 286	13 31 08.3	+30 30 32	0.849	0.692 (DLAS, 21 cm)	1994, Nov 8 1995, Nov 8	F450W F702W	2×1000 4×900	25.66 26.20
MC 1331+170	13 33 35.8	+16 49 02	2.084	0.7443 (DLAS cand.) 1.776 (DLAS, 21 cm) 1.3284 (Mg II) 1.4462 (C IV)	1995, Feb 7	F702W F814W	6×600 2×600 2×900	26.04 25.41

^a Absorption systems as currently known (see text for references)

object classification. For the detection, only two parameters have to be specified: the threshold for the detection and the parameter that controls the deblending of the objects, which depends on the dynamics of the detector. The classification of the objects is quite satisfactory, even for the slightly under-sampled images of the WFPC2. The $5\sigma_{\text{sky}}$ detection threshold, as defined in SExtractor, refers to the total flux of an object concentrated and averaged over 9 pixels, where σ_{sky} is the rms fluctuation per pixel of the background. For the PC2 sampling, this threshold corresponds to a $4\sigma_{\text{sky}}$ detection limit for an unresolved object. For all the diffuse extended objects, this selection criterion always corresponds to a detection limit of at least $2\sigma_{\text{sky}}$ or $\mu_{702,\text{lim}}=22.7$ mag arcsec⁻². The $5\sigma_{\text{sky}}$ detection threshold allows to discriminate between very faint stars and cosmic rays events, and to include low surface brightness extended objects. This leads to an average limiting magnitude $m_{702,\text{lim}} = 25.9$ for the F702W images (see Table 1). Such a value is consistent with the limit of completeness of the fields, as illustrated in Fig. 1, where we show the differential magnitude number counts of galaxies in the range $20 \leq m_{702} \leq 28$ for the seven combined fields. The dotted line indicates the counts of the deep imaging survey of Le Brun et al. (1993). The excess in the bins at magnitudes lower than 22 are statistical fluctuations due to the low number of galaxies in these bins (at most 7), while the excess between $m_{702} = 22$ and $m_{702} = 24$ may be real, and probably due to the presence of some groups near three sightlines, 3C 196, PKS 1229–021, and, at a

lower degree, Q 1209+107 (see Sects. 3.3, 3.5 and 3.4). However, the bins between $m_{702} = 24$ and $m_{702} = 26$ follow the average distribution, and the break occurring in the bin at $\langle m_{702} \rangle = 26.5$ indicates that the completeness limit of our data is about $m_{702,\text{lim}} = 26$. The complete analysis of the galaxy populations of the fields, including the WFC2 data, will be made in a subsequent paper.

All apparent magnitudes are given in these filters. For absolute magnitudes, k -corrections from observed m_{702} to rest-frame B magnitude were estimated using the templates given by Coleman et al. (1980). We used an Sbc type for all spirals discussed in the paper, and Im type for the amorphous and/or low-surface brightness galaxies. The k -corrections relative to peculiar objects (e.g the compact absorber candidates) are discussed in the text. However, elliptical types have not been considered, since the presence of large quantities of gas (ascertained by the DLAS) makes this type unlikely for these objects.

2.3. Profile subtraction

The damped Ly α absorbers are most probably located very close to the quasar sightline. Consequently, it is necessary to search for galaxies superimposed onto the quasar image. Since we have observed several quasars through the same filter, and roughly at the same location on the PC2 detector, we have been able to construct an empirical Point Spread Function (PSF). For the subtraction to the quasar image, the latter gives better results than those

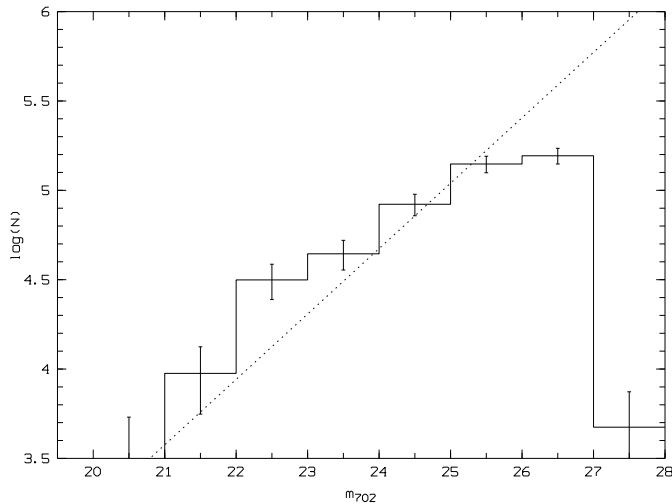


Fig. 1. Differential magnitude number counts in the cumulated seven PC2 fields. The dotted line shows the average differential magnitude counts from Le Brun et al. (1993). Note the break at the faint end, indicating the completeness limit, $m_{702,\text{lim}} \simeq 26.0$

obtained using a library of theoretical PSFs provided by the STScI.

To construct the PSF in an iterative way, we have selected for the first step the quasar field for which the candidate absorber is well resolved from the quasar image, i.e. Q 1209+107 (see Fig. 8). To obtain a first iteration clean PSF together with a reasonable sampling of the background, we have removed the image of the galaxy adjacent on the sky to the quasar image and put the corresponding pixels at the average value of the surrounding background. This initial PSF has then been used for subtraction to a second image also barely saturated, i.e. PKS 1229–021, after recentering and rescaling. The scaling factor has been estimated from the flux ratio in the wings of the quasars, excluding the saturated central pixels. As the resulting frame does not include a strong extended source close to the field center, the detected individual objects are clearly resolved from any residual pattern due to PSF subtraction. This frame has then been cleaned, all residuals but the objects being put at the average value of the background (in fact set to zero for building the PSF frames), and subsequently subtracted from the original quasar image to obtain a second PSF frame. The latter is then averaged with the initial PSF. The resulting PSF is then used to analyze the next quasar image.

We thus obtained a PSF built with four point source images of various intensities, always located close to the center of the PC2, and therefore suffering no differential optical distortions. The images of 3C 196 and 3C 286 were not used since, in both cases, there is clearly an extended underlying object that could not be properly resolved from

the PSF residuals. The image of PKS 0454+039 was not used either, because the very important residuals cannot be clearly ascribed to either the PSF or an underlying object, this being most probably due to the high saturation level of the quasar. Only the very central parts of the frames obtained after subtraction of the initial PSF show high residuals due to saturation of the final PSF. In each case, we can ascertain the existence of faint objects ($m_{702,\text{lim}} \simeq 25.2$) down to $0.3''$ from the quasar center (e.g. Q 1209+107), i.e. $2h_{50}^{-1}$ kpc at $z = 0.6$, or $0.5''$ for the most saturated quasars (e.g. EX 0302–223).

3. Description of individual fields

3.1. EX 0302–223 ($z_e = 1.4000$)

Petitjean & Bergeron (1990) have detected two metal-rich absorption systems in the spectrum of this quasar at $z_a = 0.4196$ and 1.0095 . The latter shows strong Mg II and Fe II absorption lines, and is therefore a possible DLAS. In the IUE spectrum of this quasar, Lanzetta et al. (1995) have detected Ly α absorption at $z = 1.0095$, 0.9874 and 0.9690 . The rest-frame equivalent widths w_r of each of these lines are greater than 5\AA , and each could be either damped ($N(\text{HI}) \simeq 1 \times 10^{20} \text{ cm}^{-2}$) or multiple Ly α lines. The two lower redshift systems do not have associated metal absorption lines and are thus most likely multiple Ly α -only systems, or blends of Ly α with metal lines or Galactic absorptions. A G270H FOS spectrum of EX 0302–223 will be retrievable from the HST data base in December 1996 and we will then be able to confirm the nature of the $z_d = 1.0095$ absorber. The $z_a = 0.4196$ Mg II absorber has been identified by Guillemin & Bergeron (1996, hereafter GB), with a $z_g = z_a$ very bright galaxy at a large impact parameter D , with however values consistent with the (M_R, D) scaling law given by BB91. A faint galaxy $7.7''$ away from the quasar sightline (object #7 in Table 2) has also been identified by GB at $z_g = 1.000 \simeq z_d$, but at a too large impact parameter ($D = 84.3h_{50}^{-1}$ kpc) to be the damped Ly α absorber. Finally, a Lyman limit system within 10^4 km s^{-1} from the quasar emission redshift has been detected by Koratkar et al. (1992) in a IUE spectrum, and the redshift estimated from the Lyman edge is $z_a = 1.33$.

The whole PC2 field is presented in Fig. 2 and Fig. 3 shows the $10''$ square field centered on the quasar after PSF subtraction and a Gaussian smoothing with $\sigma = 0.5$ pixel. There are four faint objects at impact parameters less than $5''$ (objects #2 to #5), the closest being detected only after profile subtraction. These objects have impact parameters smaller than 24 and $39h_{50}^{-1}$ kpc at $z = 0.4196$ and 1.0095 respectively. It is then unlikely that any of them is associated with the lower redshift Mg II absorber, since large HI column densities, thus strong Fe II absorption, are expected at such small impact parameters, but no Fe II absorption line is detected at $z = 0.4196$

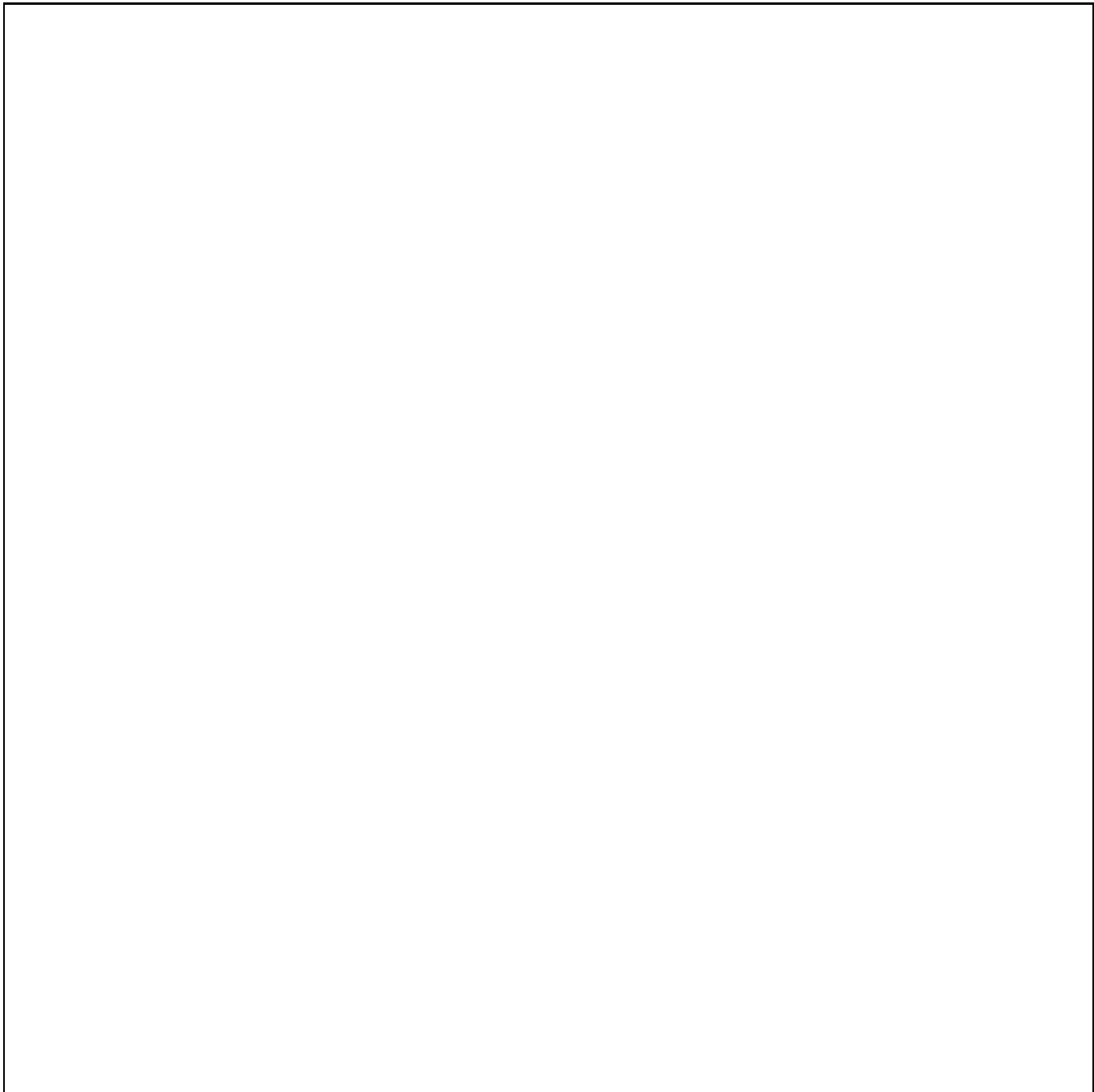


Fig. 2. Field of the PC2 around EX 0302–223 after smoothing. Objects are labeled as in Table 2

(Bergeron unpublished). Furthermore, there is no strong emission line at the wavelength of the expected [O II] λ 3727 line at $z = 1.0095$ in the spectra of objects #4 and #5, unresolved in ground-based observations (GB).

Consequently, objects #2 and #3 are the most likely damped Ly α absorber candidates, they have colors $m_{450} - m_{702} > -0.1$ and $m_{450} - m_{702} = 1.3$ respectively. Since this does not constrain their spectral types, we will use the k -correction of an Sbc galaxy. We then obtain $M_B =$

-20.4 and -22.0 for objects #2 and #3, with uncertainties as large as 0.5 mag. Object #7 would then be another field galaxy at a redshift similar to that of the damped Ly α absorber, and might contribute to the detected Mg II absorption, which is a triple system spanning 170 km s^{-1} (Petitjean & Bergeron 1990). Its absolute magnitude is $M_B = -23.4 \pm 0.5$.

The galaxies #4 and #5 are not embedded in a lower surface brightness envelope (at the 1σ rms level above the

Table 2. List of the objects in the field of EX 0302–223

Obj.	$\Delta\alpha$ "	$\Delta\delta$ "	θ "	m_{702}	m_{450}
1	0.00	0.00	0.00	17.0 ^a	16.55
2	-0.98	-0.57	1.14	25.4	-
3	-2.24	1.04	2.47	23.8	25.1
4	0.30	3.21	3.22	24.0	24.5
5	1.04	3.41	3.57	24.2	-
6	1.69	-5.47	5.73	23.63	-
7	-2.65	-7.25	7.72	22.37	-
8	-3.56	6.97	7.83	25.38	-
9	-8.36	-2.14	8.63	24.52	-
10	4.72	11.20	12.15	25.24	-
11	7.52	12.11	14.26	25.05	-
12	4.91	-13.56	14.42	24.72	-
13	-8.49	11.94	14.66	21.18	24.13
14	15.04	-0.68	15.06	18.36	19.71
15	-8.21	-12.63	15.06	25.07	-
16	-14.92	3.04	15.23	24.56	-
17	8.85	12.46	15.28	25.37	-
18	-0.11	-15.35	15.35	25.11	-
19	-5.99	15.47	16.59	25.45	-
20	11.91	-11.55	16.59	25.26	-
21	-16.35	-2.94	16.61	25.22	-
22	-14.89	8.82	17.30	22.53	23.25
23	-13.54	-10.97	17.43	25.06	-
24	-7.40	15.88	17.52	23.41	-
25	-9.65	14.87	17.73	20.52	24.25
26	15.50	-9.53	18.20	24.58	-
27	-12.34	-13.87	18.57	22.39	24.13
28	-7.40	-17.56	19.06	25.44	-

^a Saturated

background), which does not support the assumption of a physical pair. They could be associated with the strong Ly α absorbers at $z_a = 0.9874$ and 0.9690 .

There are 28 detected objects in this PC2 field brighter than the 5σ threshold or $m_{702, \text{lim}} = 25.8$. They are listed in Table 2. Object #14 is a bright, $M_B = -20.0$, fairly blue (B–R=1.3) spiral galaxy at $z = 0.118$ (Bergeron, unpublished), which should have associated Mg II absorption. This expected absorption is within the wavelength range of the FOS-G270H spectrum, not yet available in the HST archive data base. The other brighter objects in the field, #13 and #25, have very red colors, $m_{450} - m_{702} = 2.9$ and 3.7 respectively. They could be elliptical galaxies at $z \simeq 0.5$ (Frei & Gunn 1994), with impact parameters of about $110\text{--}140h_{50}^{-1}$ kpc and might have associated Ly α -only absorption. The $z = 0.4196$ absorber is thus most probably the bright galaxy identified by GB at a large impact parameter, outside the PC2 field.

3.2. PKS 0454+039 ($z_e = 1.345$)

There are two previously known absorption systems in the spectrum of this quasar. The $z_d = 0.8596$ system has very

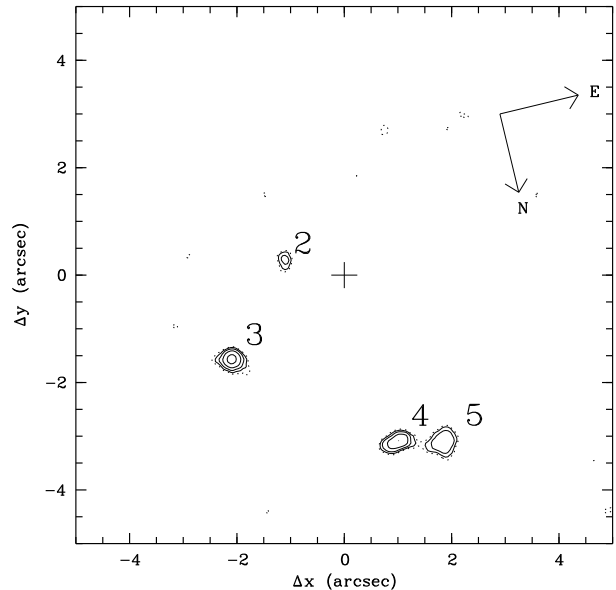


Fig. 3. Close vicinity of EX 0302–223 after PSF subtraction. The location of the quasar is marked with a cross. Contour level values are 1.5 (dotted), 2, 3, 5 and 9σ above the mean sky level

strong Mg II and Fe II absorption lines, which suggests a large $N(\text{H I})$ value. Steidel et al. (1995) have detected associated Zn II and Cr II absorption lines, which are presently found only in DLAS. They have also observed the quasar with the HST-FOS, and confirmed that the Ly α line of this system is damped with $N(\text{H I}) = 5.7 \times 10^{20} \text{ cm}^{-2}$. The $z_a = 1.1536$ system shows strong Mg II and C IV absorption, but no Fe II absorption (Steidel & Sargent 1992), and the Ly α line is clearly not damped (Steidel et al. 1995). Recently, Boissé et al. (1996) have detected two other high-redshift systems: a C IV system at $z_a = 1.0680$ and a very strong Ly α -only system ($w_r = 3.2 \text{ \AA}$) at $z_a = 0.9781$ with 8 associated lines from the Lyman series.

After PSF subtraction performed on ground-based images, Steidel et al. (1995) have detected a galaxy $2.1''$ away from the quasar, i.e. $21.7h_{50}^{-1}$ kpc at $z_d = 0.8596$, that they identified as the damped Ly α absorber. There is a bright object $4''$ east of the quasar image which is a dwarf galaxy at $z_g = 0.072$ (Steidel et al. 1993). When the color-term corrections are taken into account, our measured magnitudes for this galaxy (object #3) are in good agreement with theirs. No associated Mg II absorption has been reported by Steidel et al. (1995), but a Mg II doublet is clearly present at this redshift in the FOS-G270H spectrum obtained by Boissé et al. (1996). There is no object at small impact parameter which could give rise to the $z_a = 1.1536$ absorption system. The whole PC2 image is presented in Fig. 4 and the central part of the field is shown in Fig. 5 after PSF subtraction and smoothing. The properties of the galaxies detected in the whole PC2 field

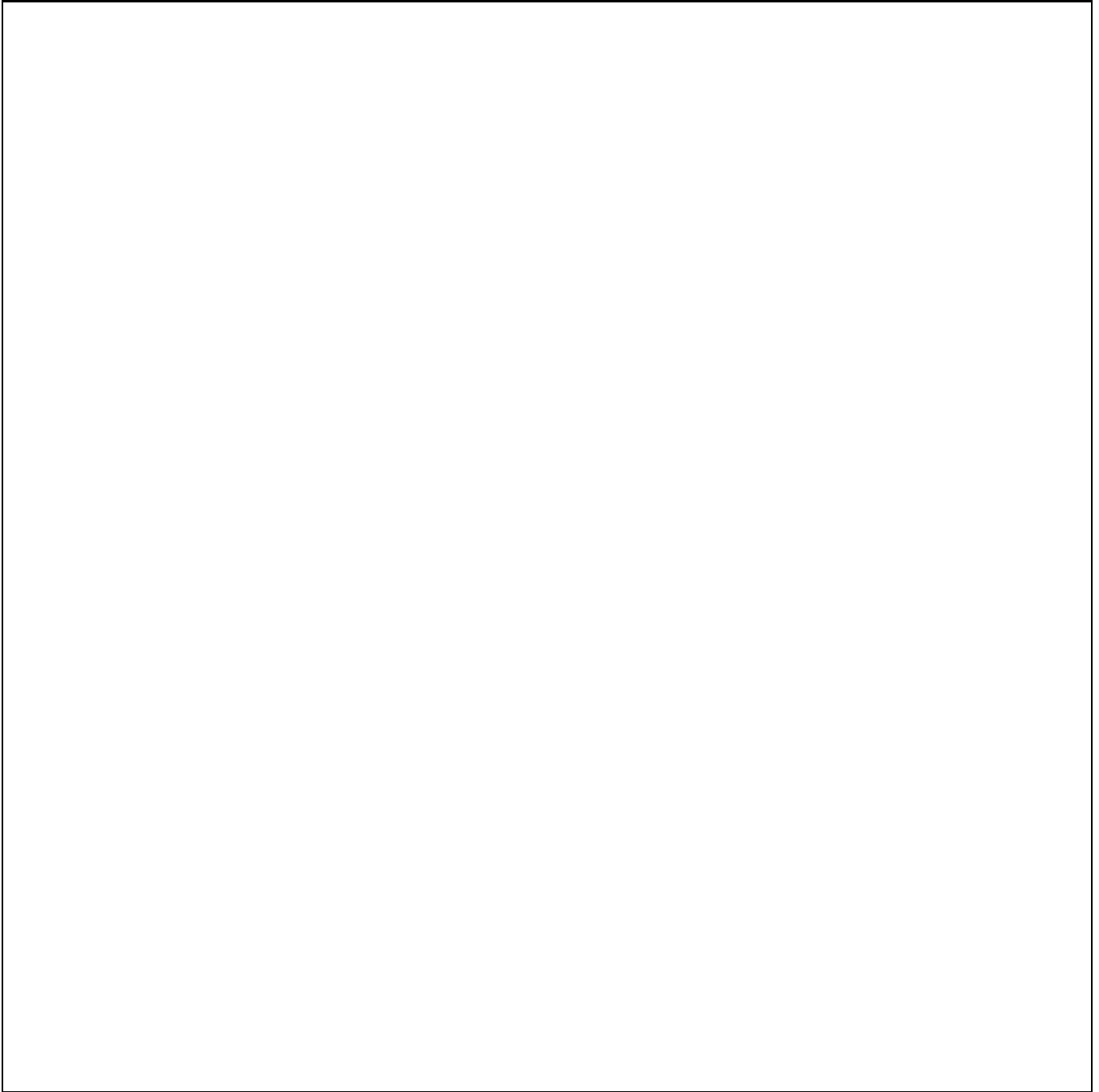


Fig. 4. Field of the PC2 around PKS 0454+039. Objects are labeled as in Table 3

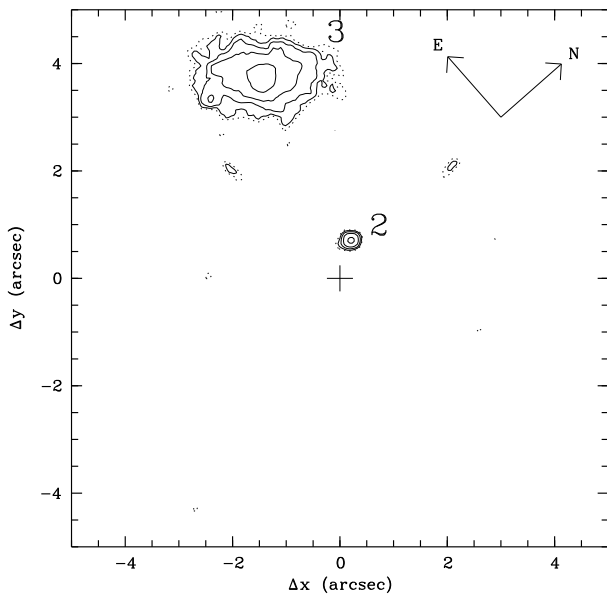
are listed in Table 3. The faint galaxy reported by Steidel et al. (1995) is just at the edge of the PC2 quasar image and very clearly detected after PSF subtraction (object #2 in Fig. 5). The impact parameter is smaller by over a factor of two than that measured by Steidel et al. (1995), most probably due to a less accurate PSF subtraction for the ground-based images; our measured R band magnitude is very close to their. Assuming this galaxy to be the damped $\text{Ly}\alpha$ absorber leads to a small

impact parameter, $D = 8.3h_{50}^{-1}$ kpc. This object is barely detected in the F450W image, near to the limiting magnitude ($m_{450} = 25.3$), and, as in the case of objects #2 and #3 in the field of EX 0302–223, we do not have any information on the spectral type of this object. Again, we use a Sbc spectrum to derive $M_B = -20.5 \pm 0.5$.

There are two galaxies in the field that could be responsible for the $z_a = 1.1536$ Mg II/C IV system: objects #4 and #5, which would then respectively have

Table 3. List of the objects in the field of PKS 0454+039

Object	$\Delta\alpha$ (")	$\Delta\delta$ (")	θ (")	m_{702}	m_{450}
1	0.00	0.00	0.00	16.61	17.64
2	0.4	0.7	0.8	24.2	25.3
3	3.79	1.43	4.05	20.31	21.55
4	4.29	4.79	6.43	25.25	-
5	0.15	-7.51	7.51	23.61	-
6	7.13	2.92	7.70	24.08	-
7	6.51	-5.82	8.74	23.05	24.90
8	9.29	0.57	9.31	22.43	23.82
9	-8.90	7.87	11.88	24.83	-
10	-11.35	-4.24	12.11	23.89	24.63
11	11.71	3.88	12.34	22.61	-
12	12.08	-7.74	14.35	23.55	-
13	-10.11	-10.33	14.45	25.18	-
14	-0.98	-15.57	15.60	24.32	-
15	-12.29	-9.90	15.78	19.63	22.65
16	-0.46	-16.12	16.12	25.57	-
17	-9.97	-15.99	18.84	23.62	-
18	-18.35	-5.29	19.10	22.60	24.19

**Fig. 5.** Same as Fig. 3 for PKS 0454+039

$M_B = -20.6$, $D = 75h_{50}^{-1}$ kpc and $M_B = -22.2$, $D = 86h_{50}^{-1}$ kpc. Object #5 is a very diffuse, irregular, low surface brightness galaxy with a peak intensity $\mu_{702,\max} = 22.7$ mag arcsec $^{-2}$. The impact parameter of object #4 is somewhat larger (by $\sim 50\%$) than the value expected for its magnitude from the (M_R, D) scaling law (BB91, GB), whereas for object #5 it is roughly equal to the maximum value given by this scaling law. Object #5 is thus tentatively identified as the $z_a = 1.1536$ absorber.

Among the 18 PC2 field objects brighter than $m_{702,\text{lim}} = 25.8$, four are classified as stars, but one of them (object #7) shows some diffuse extension suggesting a spiral arm. It is not clear whether it is a galaxy with an unresolved nucleus or a foreground star coincident with a background galaxy. There are two faint, very diffuse and extended galaxies, objects #5 (mentioned above) and #10 ($\mu_{702,\max} = 22.4$ mag arcsec $^{-2}$).

3.3. 3C 196 ($z_e = 0.871$)

Brown & Mitchell (1983) found a 21 cm absorption system in 3C 196 at $z_d = 0.437$. The associated metal lines have been identified by Foltz et al. (1988) and Boissé & Boulade (1990). Five very strong Fe II lines are detected as well as the Mn II triplet and the Ca II doublet which strongly suggests a DLAS. Since the radio emission comes predominantly from extended radio lobes, the absorber must cover both the optical quasar and part of the radio lobes, but not the more compact radio hot spot located in the northern lobe (Brown et al. 1988), and the intervening HI absorbing cloud must be larger than $4.5h_{50}^{-1}$ kpc. Finally, Oren & Wolfe (1995) have detected a substantial Faraday rotation residual toward this radio source, with $RRM = -121.8$ rad m $^{-2}$, even larger than the value derived toward the radio-jet of PKS 1229–021 by Kronberg et al. (1992). Oren & Wolfe (1995) propose that this Faraday rotation is induced by the 21 cm absorber. This quasar exhibits a second Mg II system at the quasar redshift ($z_a = 0.871$).

On high-spatial resolution images taken at the CFHT, Boissé & Boulade (1990) have detected two galaxies close to the quasar sightline (respectively at $1.2''$ and $1.7''$). They associated the brightest one to the 21 cm absorber, implying an impact parameter and absolute magnitude of $D = 12h_{50}^{-1}$ kpc and $M_R = -21.8$ (without k -correction). Cohen et al. (1996) have recently observed 3C 196 with the HST-FOS (G160L grism) and the WFC2 (pixel size of $0.0966''$, resolution of $0.15''$). Unfortunately, the Ly α line at $z_d = 0.437$ coincides with the Lyman limit system at $z_a \simeq z_e = 0.871$ and these authors could not conclude whether the $z_d = 0.437$ Ly α line is damped (with $N(\text{HI}) \simeq 1.5 \times 10^{20}$ cm $^{-2}$) or not. The latter alternative would be inconsistent with the presence of strong associated Fe II, Mn II and Ca II absorption. Their R -band images reveal that the brightest object is a barred spiral galaxy (type SBc) with very extended arms which cover the radio lobes (see their Fig. 1). As Boissé & Boulade (1990), they conclude that this object could be identified as the 21 cm/Ly α absorber, if a high column density gaseous disk is associated with this luminous spiral galaxy. In their PSF subtracted image (using a synthetic PSF generated by the Tiny Tim software) they also detect the northern, fainter object (#3 in Table 4) close to the quasar image previously reported by Boissé & Boulade (1990), which in the WFC2 image extends to approximately $1.2''$ south of the

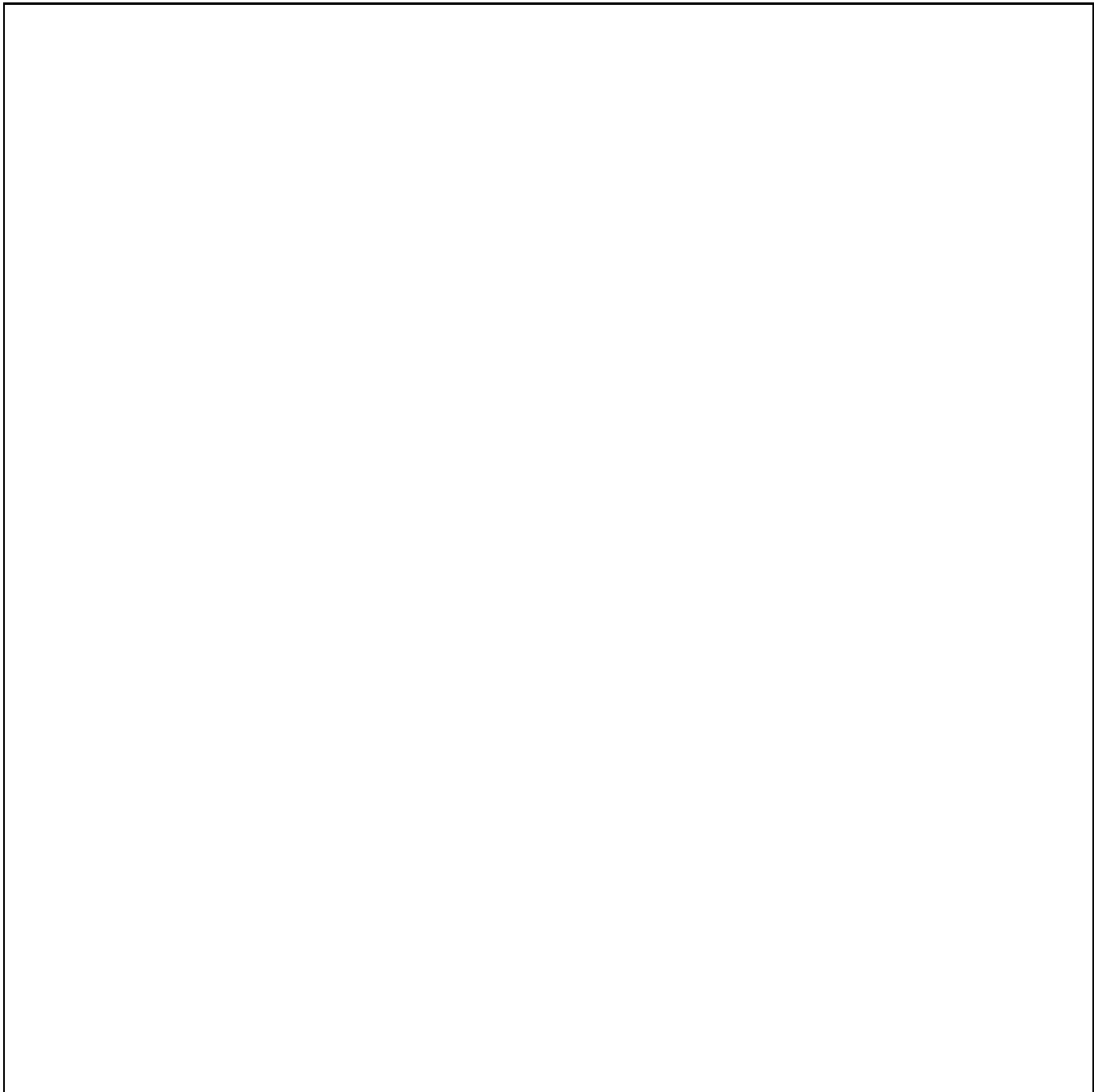


Fig. 6. Field of the PC2 around 3C 196. Objects are labeled as in Table 4

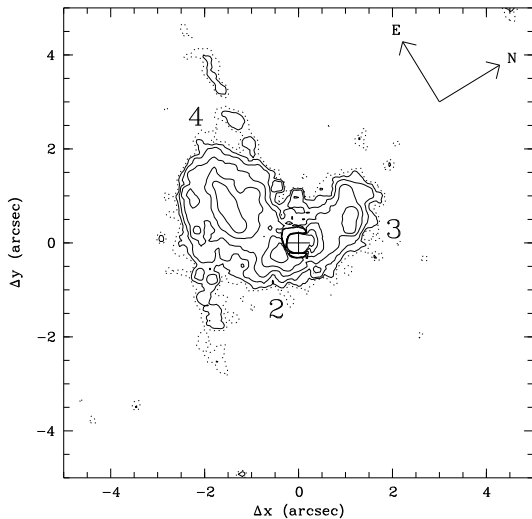
quasar. If this galaxy is at $z_g \simeq z_e = 0.871$, as suggested by Boissé & Boulade (1990), they conclude that its proximity to the quasar together with a lack of associated damped Ly α absorption would imply that either this object is not a galaxy or it is affected by the quasar ionizing radiation field. Their analysis of the $z_a \simeq z_e$ system led them to suggest that the high ionization component of this system may cover only partially the quasar emission line region,

and its physical properties could then be similar to those in BAL quasars.

Our PC2 image has a resolution about twice as high as that obtained by Cohen et al. (1996) and an exposure time in the F702W filter three times longer. We also have information on the $m_{450} - m_{702}$ color for some objects in the field, including the bar of the luminous spiral galaxy. The red image is shown in Fig. 6 and the PSF subtracted central part is given in Fig. 7 after weak smoothing. The

Table 4. List of the objects in the field of 3C 196

Object	$\Delta\alpha$ (")	$\Delta\delta$ (")	θ (")	m_{702}	m_{450}
1	0.00	0.00	0.00	17.83	18.71
2	< 0.3	< 0.3	< 0.3	< 21.25	
3	-0.3	1.1	1.1	22.3	
4	1.21	-0.86	1.48	19.96	22.23
5	1.19	2.30	2.59	24.81	-
6	2.42	6.45	6.89	22.86	24.75
7	1.97	-7.05	7.32	25.27	-
8	-7.48	-1.14	7.57	23.49	-
9	-7.12	3.00	7.73	22.04	-
10	-8.83	2.31	9.13	24.65	25.15
11	8.91	3.37	9.53	24.07	-
12	9.26	4.83	10.44	21.73	24.88
13	5.33	10.49	11.77	25.69	-
14	9.55	6.98	11.83	25.47	-
15	9.87	6.73	11.95	25.28	-
16	-1.65	-12.05	12.04	22.94	-
17	-13.16	-0.05	13.16	23.91	-
18	10.55	-8.59	13.61	23.24	-
19	10.30	8.99	13.67	24.53	25.25
20	-12.47	7.04	14.32	23.21	-
21	-9.36	-11.02	14.46	23.95	-
22	-1.75	-15.11	15.21	24.45	-
23	13.67	-8.96	16.35	22.79	-
24	4.21	16.22	16.76	22.89	-
25	-4.22	-17.25	17.76	23.52	-
26	-18.42	2.59	18.60	23.84	25.65
27	18.65	-4.72	19.24	24.08	-
28	-17.90	8.99	20.03	22.38	-
29	-20.05	1.89	20.14	25.11	-
30	-6.79	-20.01	21.14	24.61	-

**Fig. 7.** Same as Fig. 3 for 3C 196, with levels at 1.5 (dotted), 2, 3, 5, 9 and 17 and 33σ

diffuse northern object (# 3 at $\theta = 1.1''$) is clearly resolved from the quasar, whereas the southern object, reported by Cohen et al. (1996), is compact and still blended with the quasar residual image (object # 2 at $\theta \leq 0.3''$). This compact object is resolved in the north-south direction (i.e. towards the radio hot spot), but not in the east-west one. Its linear size along the major axis is roughly $1.5''$ or $16h_{50}^{-1}$ kpc at $z_g = 0.871$. This object could be related to the host galaxy of the quasar, and would then be very luminous, $M_B < -23.1$. However, this estimate is uncertain because the outermost parts of this object are blended on the southern side with the barred spiral galaxy and on the northern side with the diffuse northern object (#3). The continuum emission of the latter amorphous galaxy barely covers the northern hot spot, and not the diffuse part of the radio lobe. Object #3 could be associated with the quasar host galaxy (e.g. a tidal tail), or be a galaxy belonging to the group possibly associated with the quasar (see below). At $z_g = 0.871$, its absolute magnitude and impact parameter are $M_B = -22.0$ and $D = 11.5h_{50}^{-1}$ kpc. The interstellar medium of the galaxies #2 and #3 would then be ionized by the quasar UV radiation flux for gas densities lower than 10 cm^{-3} and radial distances up to $25h_{50}^{-1}$ kpc.

The $m_{450} - m_{702}$ color of the luminous spiral galaxy equals 2.3 and for the bar only $m_{450} - m_{702} = 2.0$. This color is that of a Sbc galaxy at redshift $z \gtrsim 0.4$ (Frei & Gunn 1994), which is consistent with this object being the 21 cm absorber. Its arms extend over $9''$ from end to end, or about $70h_{50}^{-1}$ kpc at $z_d = 0.437$. The properties of this galaxy, very large extent and high luminosity, $M_B = -22.1$, are fairly extreme for its class. In order to study its continuum spectrum and ascertain its redshift, one of us (J. Bergeron) has recently observed this object with the ARGUS integral field spectrograph at the CFHT. Data reduction are in progress, but a quick look at the time of the observing run did not reveal strong $[\text{O II}]\lambda 3727$ or $\text{H}\alpha$ emission at $z_d = 0.437$.

In the PC2 field, there are 30 objects brighter than $m_{702, \text{lim}} = 26.0$ (see Table 4). As compared to the other PC2 fields, there appears to be an excess of galaxies in the magnitude range $22.0 \leq m_{702} \leq 24.0$, statistically significant at the 4σ level. The average number of galaxies in this magnitude range is 4.2 ± 2.2 for all fields, excluding those of 3C 196 and PKS 1229–021, whereas it reaches 12 and 9 in these two latter cases (the field around PKS 1229–021 is discussed in Sect. 3.5). Since radio-loud quasars are known to lie preferentially in dense environments, this excess of galaxies most probably traces a galaxy cluster or group associated with 3C 196. The average absolute magnitude of the cluster galaxies detected in the PC2 field is $M_B \simeq -21.4$. A preliminary analysis of the WFC2 adjacent fields gives a similar 4σ excess as compared to the expected average number density of galaxies per magnitude and per square degree (see e.g. Le Brun et al. 1993) over a

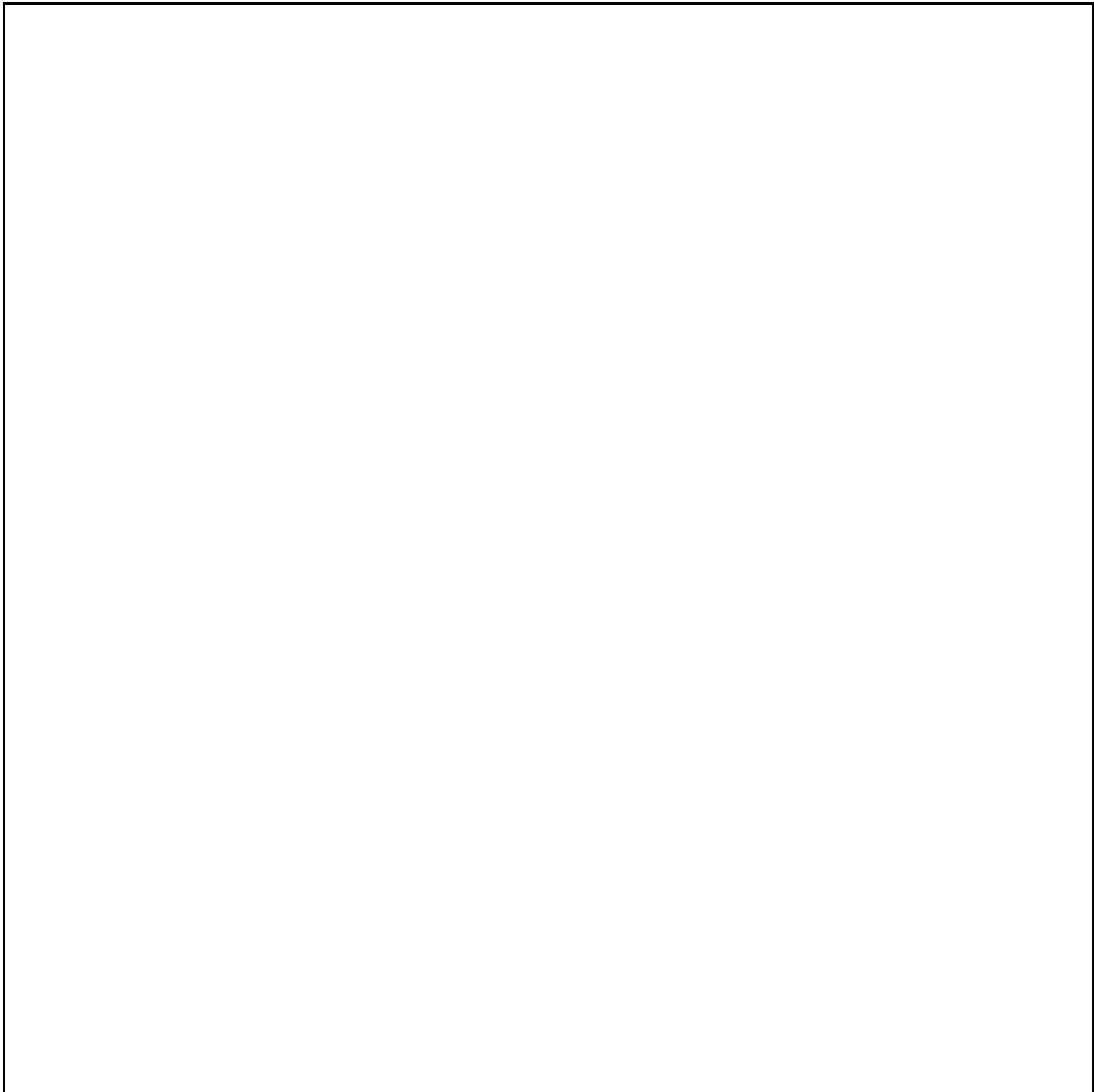


Fig. 8. Field of the PC2 around Q 1209+107. Objects are labeled as in Table 5

similar range of apparent magnitudes, $22.0 \leq m_{702} \leq 24.5$, or $-23.6 \leq M_B \leq -20.6$ at $z_e = 0.871$.

3.4. Q 1209+107 ($z_e = 2.191$)

This quasar exhibits three absorption systems at $z_a = 0.3930$ (Mg II), 0.6295 (strong Mg II and Fe II) and 1.8434 (Mg II) (Young et al. 1982). A galaxy at an angular impact parameter $\theta = 7.1''$ and with a magnitude $m_R = 21.9$

has been identified by Cristiani (1987) as the $z_a = 0.3930$ absorber. In high spatial resolution CFHT images, Arnaud et al. (1989) have detected a galaxy at $1.3''$ from the quasar sightline, which corresponds to $11.8h_{50}^{-1}$ kpc at $z_d = 0.6295$. This small impact parameter together with the low ionization level of the $z_d = 0.6295$ absorber, strongly suggest that the Ly α line of this system is damped. Boissé et al. (1996) have observed this quasar with the HST-FOS and detected a strong Ly α absorp-

Table 5. List of the objects in the field of Q 1209+107

Object	$\Delta\alpha$ (")	$\Delta\delta$ (")	θ (")	m_{702}	m_{450}
1	0.00	0.00	0.00	18.06	18.63
2	1.62	-0.10	1.62	21.59	23.07
3	-5.34	1.03	5.43	20.10	23.68
4	-5.04	2.65	5.70	23.89	-
5	5.89	-3.34	6.77	25.37	-
6	-6.66	-1.87	6.91	25.00	-
7	-3.93	-5.77	6.98	23.53	-
8	5.35	4.81	7.20	21.66	22.73
9	4.49	5.78	7.32	22.23	23.48
10	8.66	-4.07	9.57	25.18	-
11	-4.75	8.78	9.99	22.83	24.65
12	11.34	-2.19	11.55	24.58	-
13	0.87	-11.70	11.73	25.28	-
14	-4.54	-11.63	12.49	25.06	-
15	12.55	-0.40	12.56	23.58	-
16	10.47	8.00	13.18	24.54	-
17	-13.44	6.95	15.13	24.73	-
18	-7.32	13.29	15.17	24.96	-
19	14.96	3.91	15.46	25.31	-
20	11.20	10.68	15.48	23.99	25.41
21	-5.17	15.36	16.20	24.63	-
22	-3.63	-16.08	16.49	24.04	-
23	10.99	12.52	16.66	24.25	-
24	11.77	12.43	17.12	24.09	25.60
25	-7.91	-16.59	18.38	24.44	-
26	18.33	-4.84	18.96	24.11	25.55
27	15.36	-12.99	20.12	25.10	-
28	-18.38	9.04	20.48	24.35	-

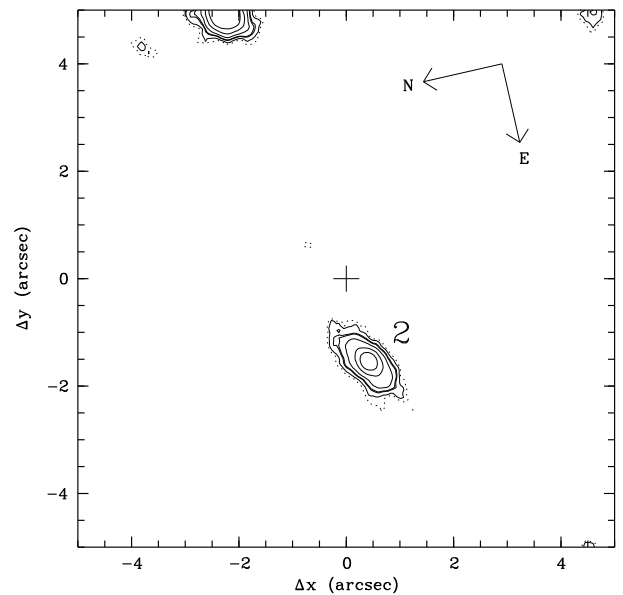
tion with $w_r = 12 \text{ \AA}$. The complex line profile does not however permit to unambiguously conclude that this line is damped. In the assumption of a damped line, the HI column density would reach $3 \times 10^{20} \text{ cm}^{-2}$.

The PC2 field of Q 1209+107 is shown in Fig. 8. The galaxy detected by Arnaud et al. (1988) is well resolved from the quasar image (object #2). After PSF subtraction, there is no closer object to the quasar sightline down to an impact parameter $\theta = 0.3''$ and apparent magnitude $m_{702} = 25.2$ (see Fig. 9). Consequently, we identify this galaxy as the $z_d = 0.6295$ absorber. The galaxy rest-frame magnitude is $M_B = -22.0$, and its projected distance to the quasar sightline equals $D = 14.5h_{50}^{-1} \text{ kpc}$. Its color, $m_{450} - m_{702} = 1.5$, is compatible with that of a spiral galaxy at intermediate redshift (Frei & Gunn 1994). The galaxy major and minor axes are equal to $2.03''$ and $0.75''$, leading to linear sizes of 18.4 and $6.8h_{50}^{-1} \text{ kpc}$ and an inclination angle of about 70 deg . The quasar sightline intersects the disk of the galaxy at a radial distance of $28h_{50}^{-1} \text{ kpc}$.

The object located $7''$ north-east to the quasar sightline, and identified by Cristiani (1987) as the $z_a = 0.3930$ absorber, is resolved into two well separated galaxies in

our PC2 image (#8 and #9). Both galaxies are very blue, $m_{450} - m_{702} = 1.1$ and 1.3 for objects #8 and #9 respectively, which suggests an interactive pair, their projected linear separation being then equal to $10h_{50}^{-1} \text{ kpc}$. The elongated, bright central parts of galaxy #9 are embedded in a diffuse extended envelope. Recent integral field spectroscopic observations at CFHT by one of us (J. Bergeron) show that the very strong optical line emission detected by Cristiani (1987) is due to object #8.

There are three possible candidates for the $z_a = 1.8434$ C IV absorber, all having diffuse and irregular morphologies: object #4 ($D = 73h_{50}^{-1} \text{ kpc}$, $M_B = -22.8$), which is close to a bright star (object #3), object #7 ($D = 90h_{50}^{-1} \text{ kpc}$, $M_B = -23.1$), and object #11 ($D = 129h_{50}^{-1} \text{ kpc}$, $M_B = -23.8$). All three candidates would then be very luminous galaxies.

**Fig. 9.** Same as Fig. 3 for Q 1209+107, with levels 1.5 (dotted), 2, 3, 5, 9 and 17σ

3.5. PKS 1229–021 ($z_e = 1.038$)

In the quasar radio spectrum, Brown & Spencer (1979) have discovered a 21 cm absorption system at $z_d = 0.39498$, and associated metal lines of Mg II, Fe II, Ca II and Mg I have been detected by Briggs et al. (1985). This system may include up to 13 components spread over 250 km s^{-1} (Lanzetta & Bowen 1992). Another Mg II system at $z_a = 0.7568$ (Steidel et al. 1994a) has an associated Lyman Limit discontinuity discovered in the IUE spectrum of the quasar (Lanzetta et al. 1992), which appears roughly at the expected wavelength for the $z_d = 0.39498$ Ly α line. Nevertheless, the recent HST-FOS spectrum of Boissé et al. (1996) clearly indicates that the latter line

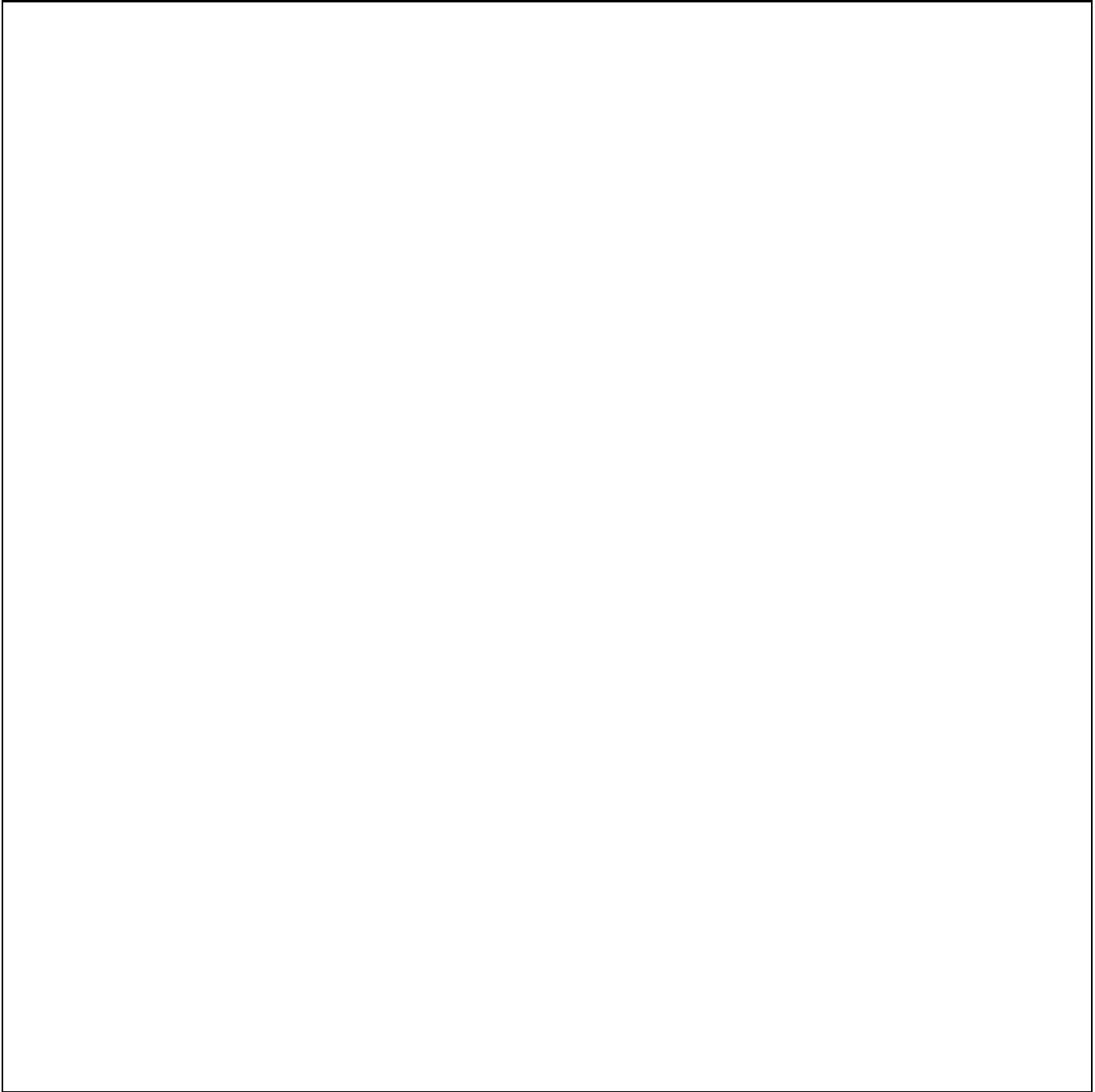


Fig. 10. Field of the PC2 around Q 1229–021. Objects are labeled as in Table 6

is damped with $N(\text{H I}) \simeq 4 \times 10^{20} \text{ cm}^{-2}$ (this was not *a priori* obvious since the radio and optical sources do not coincide spatially). These data also reveal an additional C IV system at $z_a = 0.7005$. The 21 cm absorber has not been identified by BB91, who concluded that it should be very close ($\theta \leq 1''$) to the quasar sightline, as expected from the presence of 21 cm absorption. By measuring the Faraday rotation of the radio emission along the radio jet that extends to about $3''$ west to the quasar, and using

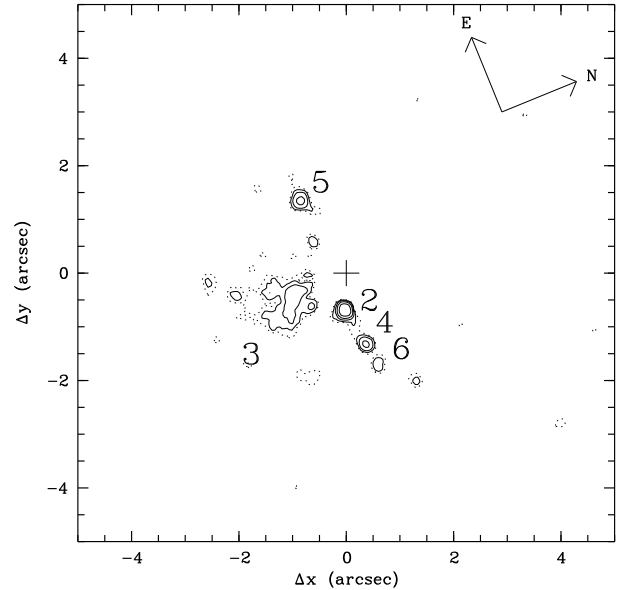
a model of the magnetic field of a spiral galaxy, Kronberg et al. (1992) concluded that the observed Faraday rotation was compatible with an intervening spiral galaxy being located $2''$ south-west to the quasar sightline. After PSF subtraction performed on ground-based images of this quasar, Steidel et al. (1994a) have found two objects within $2''$ from the quasar image. They have associated the brightest southern object to the DLAS, and the eastern galaxy to the higher redshift absorber.

Table 6. List of the objects in the field of PKS 1229–021

Object	$\Delta\alpha$ (")	$\Delta\delta$ (")	θ (")	m_{702}	m_{450}
1	0.00	0.00	0.00	16.89	17.65
2	-0.6	-0.2	0.6	24.2	24.4
3	0.3	-1.4	1.4	23.0	-
4	-1.4	-0.1	1.4	25.0	-
5	1.6	-0.3	1.6	25.1	-
6	-1.8	-0.1	1.8	25.8	-
7	-6.76	-3.88	7.80	24.88	-
8	-7.97	0.69	8.00	24.61	-
9	-4.61	6.88	8.28	22.66	-
10	-4.40	7.86	9.01	22.11	23.20
11	-3.88	-8.79	9.61	22.89	-
12	-7.90	7.06	10.59	24.58	-
13	-5.59	10.35	11.77	25.31	-
14	10.32	-7.01	12.47	23.91	24.37
15	12.42	2.92	12.76	25.43	-
16	11.87	6.68	13.62	24.93	-
17	-2.06	13.60	13.75	22.60	-
18	0.78	-15.82	15.84	23.57	-
19	14.88	-6.23	16.13	24.55	-
20	8.27	14.53	16.72	22.73	-
21	9.55	-14.74	17.56	25.45	-
22	-12.04	12.94	17.67	24.79	-
23	-17.95	1.96	18.06	24.97	-
24	5.19	17.89	18.62	23.12	-
25	-2.99	-19.41	19.64	23.02	24.33
26	-18.00	10.85	21.02	24.80	-
27	-19.45	9.19	21.52	24.30	-
28	-21.09	7.82	22.49	23.99	-

The PC2 field around PKS 1229–021 is presented in Fig. 10. After PSF subtraction, we have discovered five objects very close to the quasar sightline (see Fig. 11 and Table 6). The southern object (#3) detected in our CFHT images and by Steidel et al. (1994a) is a very diffuse irregular galaxy with a peak intensity $\mu_{702,\max} = 23.2$ mag arcsec $^{-2}$. From the PC2 data, we get a magnitude $m_{702} = 23.1$ and an impact parameter $\theta = 1.4''$. If identified as the damped Ly α absorber, it has $M_B = -18.9$ and $D = 9.9h_{50}^{-1}$ kpc. This absorber would then be fairly faint. However, due to its very small pixel size, the PC2 is not very sensitive to low surface brightness emission, and the magnitude derived from our CFHT data is brighter, $m_R = 22.1$ and probably more reliable. That measured by Steidel et al. (1994a) in the I -band is also high, $m_I = 21.7$.

The other four objects at small impact parameters are compact: one (#5) is east to the quasar and the other three (#2, #4 and #6, all unresolved), are well aligned. Object #2 is also detected in the F450W image and is very blue with $m_{450} - m_{702} = 0.2$. This alignment draws our attention onto a possible relationship with the radio jet. Indeed, the superposition of our F702W image on a recent higher resolution 8.16 MHz radio map that Dr. P.

**Fig. 11.** Same as Fig. 3 for PKS 1229–021, with levels 1.5 (dotted), 2, 3, 5, 9 and 17σ

Kronberg kindly communicated to us (unpublished observations by Kronberg, Perley, Dyer & Roeser), shows a remarkable correspondence between objects #2, #4, #6 and the three first radio knots seen along the radio jet (see Fig. 12). This quasar is then one of the very few sources, and to our knowledge the one with the highest redshift, for which optical emission associated to a radio jet has been seen. It bears some resemblance to e.g. 3C 277.3 (Miley et al. 1981; Bridle et al. 1981) and 3C 346 (Dey & van Breugel 1994; van Breugel et al. 1992) in the sense that optical emission arises preferentially at locations where the jet shows a break. In particular, PKS 1229–021 appears unlike 3C 78 in which the spatial distribution of the optical emission is continuous and closely follows the unbent radio jet. Clearly, the presence of the three radio/optical knots is closely connected to the radio source morphology. At the brightest object #2, the jet strongly interacts with some material and is deflected northward while, further away from the central core, the jet is deflected southward in a more continuous manner until it joins the south-west lobe. On the contrary, the (undetected) north-east flow expands more freely. Regarding the origin of the absorption systems, it therefore appears that none of objects #2, #4 and #6 can be considered as candidate absorbers. However, the emitting gas with which the jet interacts may be responsible for the Faraday rotation observed by Kronberg et al. (1992), especially since no galaxy-like object is seen towards the jet. Blob #2, which is the closest ($\theta = 0.6''$ or $D = 6.6h_{50}^{-1}$ kpc at $z_e = 1.038$) and the bluest object, could correspond to a cloud belonging to the galaxy hosting PKS 1229–021 on which the jet rebounds while the furthest away blobs could be associated

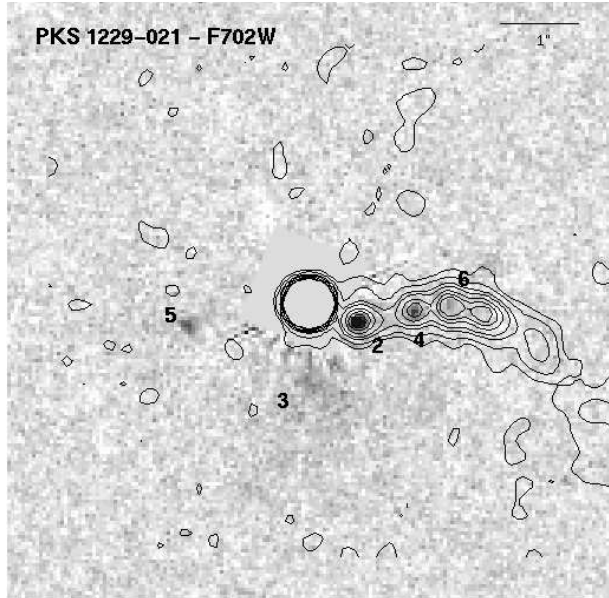


Fig. 12. $8'' \times 8''$ field around PKS 1229–021, with the contours of the radio jet (Kronberg, private communication), which shows the alignment of objects #2, 4 and 6 along the jet. North is up and east is to the left

with gas entrained outside this galaxy by the jet. Assuming a flat spectrum, these three blobs have absolute rest frame magnitudes $M_B = -20.4$, -19.6 and -18.7 for #2, #4 and #6 respectively.

The eastern compact blob #5 may cause either the $z_a = 0.7568$ system (as suggested by Steidel et al. 1994a; this Mg II absorber would then have a magnitude $M_B = -18.8$), or the $z_a = 0.7005$ C IV absorption system.

There are 28 objects brighter than $m_{702, \text{lim}} = 25.8$ in this field (Fig. 10 and Table 6). There is a 3σ level excess of galaxies in the magnitude range $22 \leq m_{702} \leq 24$, which may trace a group or a cluster of galaxies at the quasar redshift ($z_e = 1.038$). This magnitude range corresponds to $-24.1 \leq M_B \leq -22.1$ at this redshift. As for 3C 196, the analysis of the WFC2 data will provide further information on this galaxy excess. We note that Steidel et al. (1994a) also discovered several galaxies with optical and IR colors consistent with the assumption of a cluster of elliptical galaxies at the quasar redshift.

In ground-based images, objects #9 and #10 are totally blended (BB91; Steidel et al. 1994a), but are clearly separated on the PC2 images. Object #10 is bright and compact, and object #9 is fainter and very diffuse. It is most likely that the optical emission lines detected at $z = 0.199$ by BB91 arise from the brightest object, which would then have absolute magnitude $M_B = -18.5$. Its impact parameter is $D = 37h_{50}^{-1}$ kpc, nearly twice as large as the value predicted by the luminosity-halo radius scaling-law derived by BB91 for Mg II absorbers, which is consistent with the non-detection in the HST-FOS quasar spec-

trum of an associated Mg II absorption (Boissé et al. 1996). Object #11 is very red, $m_{450} - m_{702} > 2.3$, and could be an elliptical galaxy at $z \simeq 0.2$.

3.6. 3C 286 ($z_e = 0.849$)

Table 7. List of the objects in the field of 3C 286

Object	$\Delta\alpha$ "	$\Delta\delta$ "	θ "	m_{702}	m_{450}
1	0.00	0.00	0.00	16.84	17.99
2	< 0.3	< 0.3	< 0.3	< 21.3	
2a	0.1	-0.4	0.4	21.8	24.1
2b	0.2	0.4	0.4	22.4	25.2
2c	0.9	0.0	0.9	22.8	-
3	0.9	1.7	1.9	25.6	-
4	0.99	5.51	5.60	25.40	-
5	-4.03	7.26	8.30	23.38	-
6	7.53	-3.68	8.38	24.58	25.65
7	-8.18	2.09	8.44	22.71	-
8	-7.23	-4.58	8.56	25.26	-
9	-3.83	-7.84	8.73	25.58	-
10	-1.99	8.53	8.76	24.09	-
11	-8.87	1.49	9.00	25.23	-
12	-7.28	6.25	9.60	24.49	-
13	9.47	-3.03	9.95	24.66	-
14	10.72	1.79	10.87	21.01	24.45
15	-4.15	10.19	11.00	24.58	-
16	11.13	-1.98	11.30	25.79	-
17	-7.11	-10.21	12.44	25.75	-
18	-14.02	0.06	14.02	23.61	25.45
19	-14.15	3.40	14.55	25.06	-
20	-5.58	13.80	14.89	23.28	24.59
21	-14.90	-1.97	15.03	25.70	-
22	-5.13	14.31	15.20	25.83	-
23	10.85	-11.30	15.67	25.36	24.49
24	-6.07	14.67	15.88	25.73	-
25	-2.13	16.15	16.29	25.31	-
26	-6.75	14.88	16.34	25.73	-
27	15.40	-7.21	17.01	25.42	-
28	-2.47	16.86	17.04	24.92	24.45
29	17.14	-4.23	17.65	24.68	-

A 21 cm absorption line was detected at $z_d = 0.692$ by Brown & Roberts (1973), and shows a single, narrow ($b = 5 \text{ km s}^{-1}$) component. The associated Mg II and Fe II lines have been observed by Spinrad & McKee (1979). Using Pre-COSTAR FOS observations, Cohen et al. (1994), have shown that the Ly α line is damped, and their estimate of the H I column density is $\simeq 2 \times 10^{21} \text{ cm}^{-2}$. Using this value and their own measurements of Fe II, Zn II and Cr II, Meyer & York (1992) derived a very low metal abundances of $Z_{\odot}/17$, for a look back time comparable to the age of our solar system. Steidel et al (1994a) have obtained ground-based broad-band images of this quasar, and after PSF subtraction, they detected a galaxy of low surface

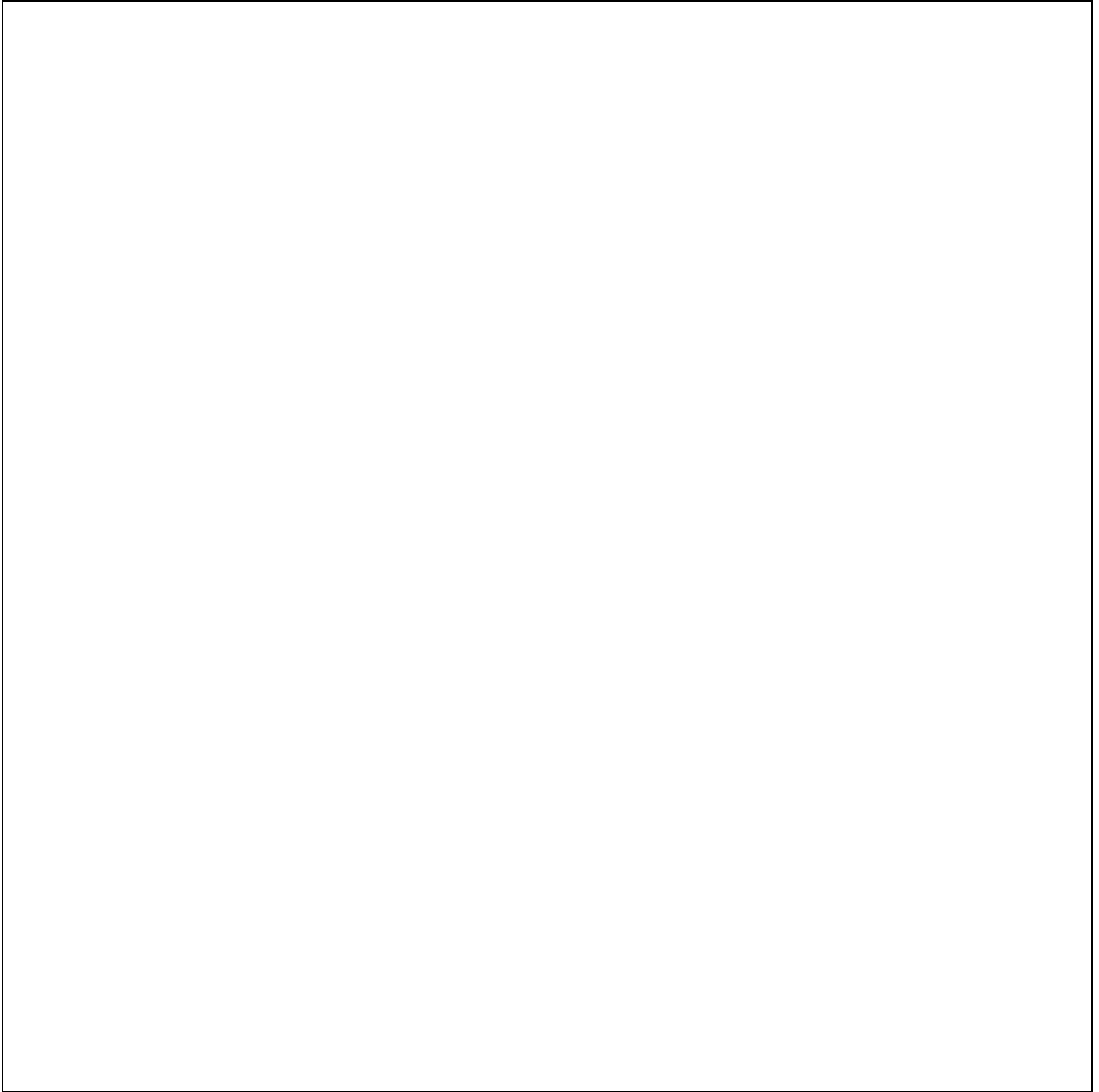


Fig. 13. Field of the PC2 around 3C 286. Objects are labeled as in Table 7

brightness, $\mu(I_{AB}) = 25.5 \text{ mag arcsec}^{-2}$, $2.5''$ away from the quasar sightline. If at the absorption redshift, its linear impact parameter would be $D = 24h_{50}^{-1} \text{ kpc}$. Furthermore, Steidel et al. (1994a), claimed that this low surface brightness could explain the low metallicity of the absorber since (according to e.g Mc Gaugh 1994), low-surface brightness galaxies have a slower chemical evolution than “normal” galaxies as the Milky Way.

In Fig. 13, we show the PC2 field around 3C 286. At the location of the object detected by Steidel et al. (1994a), $2.5''$ south-east to the quasar sightline, we do not detect any extended emission, most probably because PC2 observations are not as sensitive to low surface brightness emission as ground-based images. However, south-east to the quasar image, aside from a very faint object (object #3 in Fig. 14), with $m_{702} = 25.6$ and an impact parameter of $1.9''$ we detect diffuse emission that we identify with

the inner part of Steidel et al.’s amorphous object. After quasar profile subtraction, we do find a very bright object roughly centered on the quasar (see Fig. 14). There are two main components along the south-north axis (labeled #2a and #2b), and a bright extension of lower surface brightness at the south-east (#2c). It is possible that all these components belong to the damped Ly α absorber, and its magnitude would then be $M_B < -22.0$. A possible alternative is that objects #2a and #2b, which are located roughly symmetrically to the quasar, are both part of the quasar’s host galaxy, which central region lies on the saturated part of the quasar image, while object #2c is the damped Ly α absorber. There is some spatial over-

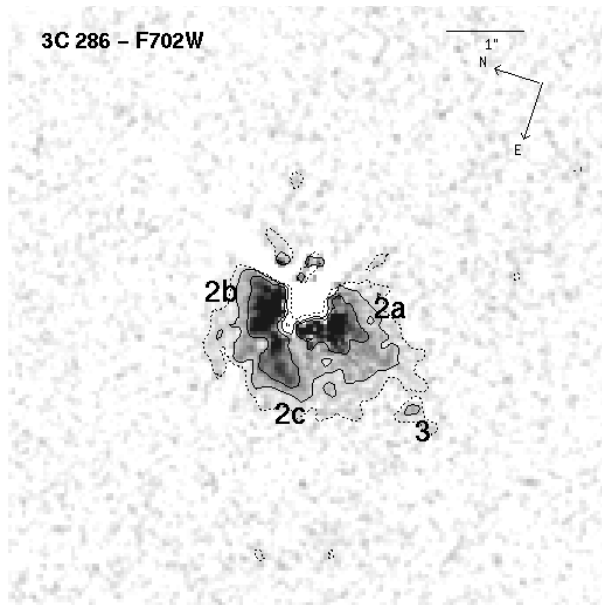


Fig. 14. $10'' \times 10''$ field around 3C 286, showing the objects as labeled in Table 7. The 1.5σ (dotted) 3σ and 7σ level contours have been overlotted

lap between the object found by Steidel et al. (1994a) and the diffuse emission detected in our PC2 image south of object #2c. The latter could also have a western extension blended with the quasar image residuals. This would be required to account for the 21 cm absorption, since more than 90% of the radio emission arises from the core of the source (Spencer et al. 1991 and references therein). Identifying object #2c as the damped Ly α /21 cm absorber leads to a magnitude $M_B = -20.5$ and an impact parameter $D = 8.5h_{50}^{-1}$ kpc. The magnitude of the quasar’s host galaxy would then be brighter than $m_{702} = 21.8$, thus $M_B < -22.3$.

There are 29 objects brighter than $m_{702, \text{lim}} = 26.2$ in the PC2 field around 3C 286 (Fig. 13). The most peculiar is object #14, which has a very elongated disturbed morphology, with a length of $3''$ and a width of $0.71''$, a peak surface brightness $\mu_{702, \text{max}} = 22.3$ mag arcsec $^{-2}$,

and a very red color, $m_{450} - m_{702} = 3.4$. This object shows three emission lines ([O II] $\lambda 3727$ and [O III] $\lambda\lambda 4959, 5007$) at $z = 0.3338$, which leads to $D = 68h_{50}^{-1}$ kpc and $M_B = -20.0$ (Le Brun et al. 1997).

3.7. MC 1331+170 ($z_e = 2.084$)

There are four certain, metal-rich absorption systems detected in the spectrum of this quasar, of which two are multiple. The lowest redshift system is double, $z_d = 0.7443, 0.7454$, which corresponds to a velocity separation of 170 km s $^{-1}$; both components show Mg II and Fe II absorption lines (Sargent et al. 1988), indicative of a DLAS. In the high spectral resolution data of Churchill et al. (1995), there are in fact six components, including the two quoted above, spread over 470 km s $^{-1}$, and symmetrically disposed. This is typical of a radial inflow/outflow (Churchill et al. 1995), or a disk seen edge-on. The existence of a strong DLAS at higher redshift prevents observation of the Ly α line from this system. There is a strong Mg II doublet at $z_a = 1.3284$, blended with the Fe II $\lambda 2344$ lines at $z_a = 1.776, 1.786$ (Steidel & Sargent 1992). Sargent et al. (1988) detected a CIV doublet at $z_a = 1.4462$, too faint to be included in the sample of Young et al. (1982), and these are the only lines seen at this redshift. The $z_a = 1.786$ component of the high-redshift double system shows strong CIV and Mg II absorption, whereas that at $z_d = 1.776$ has been detected in 21 cm (Wolfe & Davis 1979) and has an associated damped Ly α absorption from which Chaffee et al. (1988) derived an HI column density of 1.5×10^{21} cm $^{-2}$. There are 32 lines associated with this system, from C I and O I to C IV and Si IV, and the derived carbon abundance is similar to the Galactic value. The $z_a = 1.786$ system exhibits Mg II and Fe II absorption, but no associated 21 cm absorption.

High spatial resolution images taken at CFHT (Churchill et al. 1995; Bergeron unpublished) show several faint objects around the quasar sightline. Among these, there is an edge-on spiral galaxy $2''$ from the quasar sightline and with its major axis nearly aligned with the quasar sightline. This favorable geometry, the brightness of the galaxy and the velocity splitting of the lower redshift DLAS candidate led us to tentatively identify this object as the $z_d = 0.7443$ absorber prior to the results of this HST survey. No redshift is available for any of these objects.

Since there is a confirmed DLAS at high redshift, images were taken in the F702W and F814W filters (the latter corresponds roughly to the standard I filter). The F702W filter image of the PC2 is presented in Fig. 15. After PSF subtraction, the HST images reveal one faint object very close to the quasar sightline (object #2 in Fig. 16), at an impact parameter $\theta = 0.75''$ and with a magnitude $m_{702} = 24.9$. The other objects (#3 to #5) that appear on Fig. 16 were already visible before PSF subtraction (Fig. 15). We have also removed the quasar

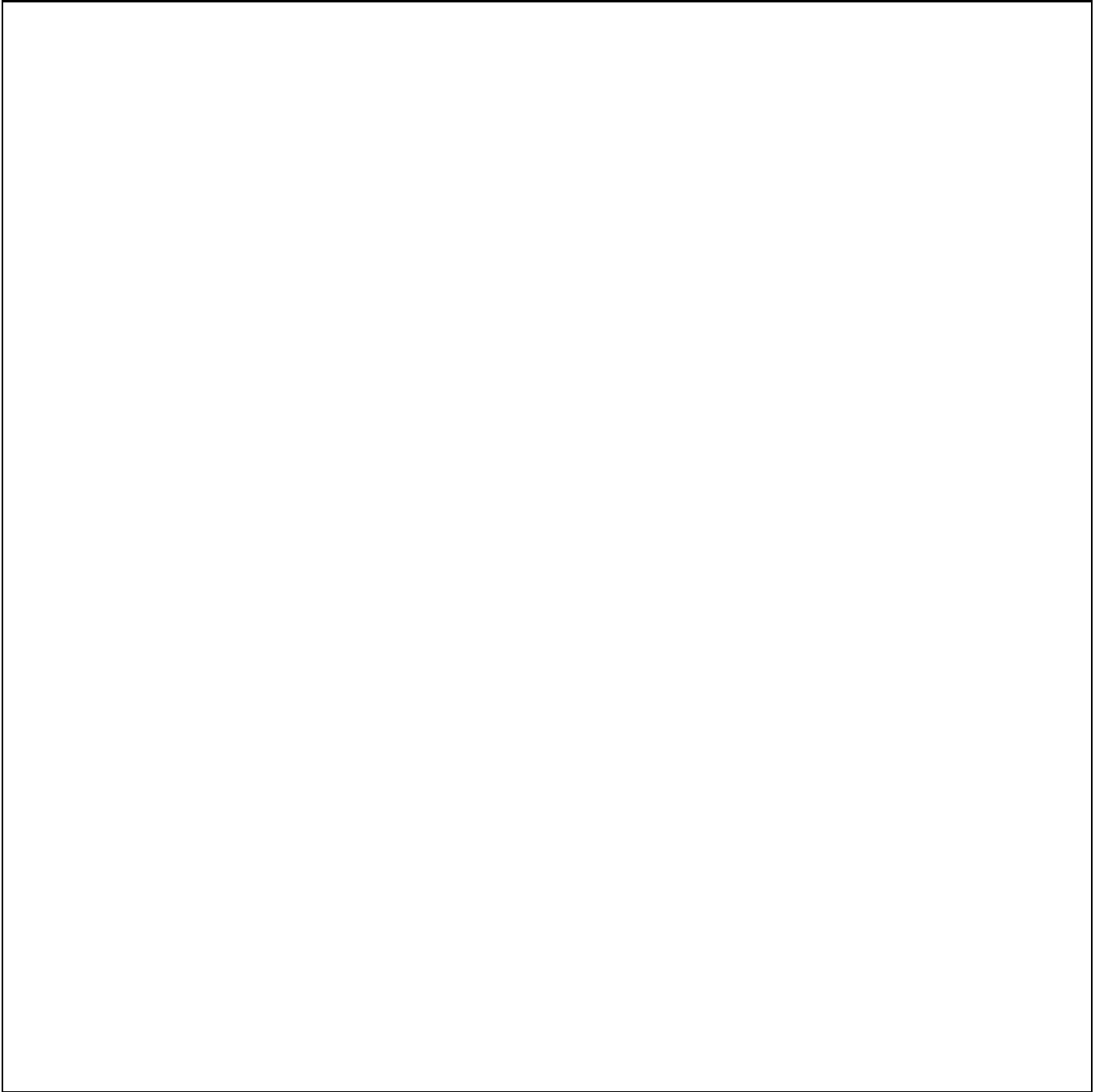


Fig. 15. Field of the PC2 around MC 1331+170. Objects are labeled as in Table 8.

image on the F814W frame using the PSF derived for the F702W images. Even if the shape of the PSF is color dependent, the resulting image is adequate for object detection at impact parameters $\theta \geq 0.6''$. Object #2 is clearly detected in the F814W image, but the estimate of its magnitude is uncertain due to important PSF residuals from the quasar image. The two closest objects (#2 and #3) could be at $z \simeq 1.78$, may be part of a group, and give rise to the $z_d = 1.776$ and $z_a = 1.786$ absorption systems.

They would then have impact parameters $D = 9.5h_{50}^{-1}$ kpc and $20.0h_{50}^{-1}$ kpc and magnitudes $M_B = -23.0$ and -22.7 respectively (note however that the k -correction needed to estimate the rest-frame B magnitude is quite large at this redshift even for the F814W data (1.7 mag), and that the uncertainty is about 0.5 mag). Object #4 would be intrinsically very luminous, unless it were at $z_d = 0.7443$. If it is identified as the $z_a = 1.3284$ absorber, its magnitude and impact parameter would be $M_B = -23.6$, $D = 34h_{50}^{-1}$ kpc,

Table 8. List of the objects in the field of MC 1331+170

Object	$\Delta\alpha$ (")	$\Delta\delta$ (")	θ (")	m_{702}	m_{814}
1	0.00	-0.00	0.00	16.91	16.55
2	0.58	0.48	0.75	24.9	23.8 ^a
3	-0.90	-1.30	1.58	25.1	24.4
4	2.82	0.50	2.86	24.2	24.2
5	-1.53	-3.54	3.86	21.40	21.47
6	2.53	6.61	7.08	25.50	-
7	-5.27	5.21	7.41	25.44	25.12
8	-2.13	-7.54	7.84	25.47	24.50
9	-6.35	-4.96	8.06	24.37	23.82
10	7.79	-3.23	8.43	25.73	24.36
11	-6.39	7.88	10.14	25.06	25.29
12	-10.99	-0.52	11.00	24.94	24.92
13	-10.47	-4.87	11.55	24.96	24.66
14	-3.80	-11.17	11.80	24.21	24.17
15	6.39	10.79	12.54	25.57	-
16	-7.21	-10.82	13.01	25.62	-
17	0.19	-13.38	13.38	25.71	-
18	13.94	-7.25	15.71	25.61	-
19	-11.63	-11.02	16.02	25.82	24.60
20	15.81	5.07	16.60	25.49	25.11
21	-15.41	-7.80	17.27	24.76	23.99
22	18.21	2.28	18.36	25.02	24.58
23	2.54	18.37	18.55	25.10	25.16
24	19.33	-0.02	19.33	24.76	24.50
25	20.04	-1.15	20.08	24.36	24.22
26	2.45	-20.57	20.71	25.86	-

^a The error on the magnitude of this object may be large, since it is partly located in a region where subtraction residuals are present

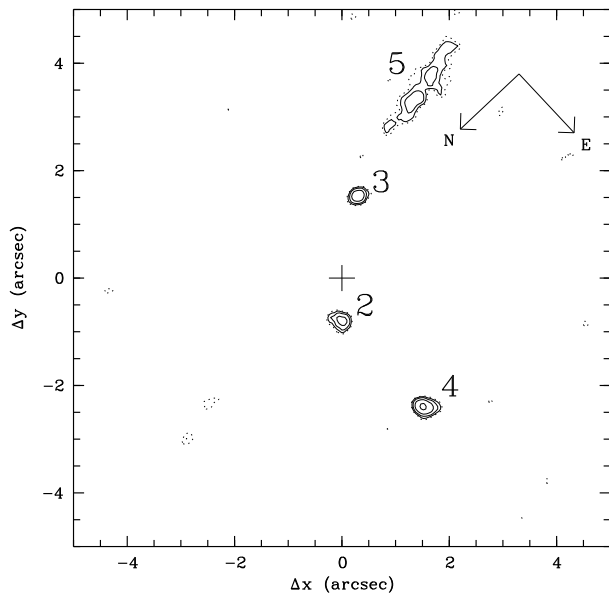


Fig. 16. Same as Fig. 3 for MC 1331+170, with levels 1.5 (dotted), 2, 3, 5 and 9σ

i.e. within the range found for lower redshift Mg II absorbers, although on the bright end. The $z_a = 1.4462$ C IV absorption could be produced by any one of the objects #6 to #10. Their absolute magnitudes and impact parameters would then be within the ranges $-22.0 \leq M_B \leq -20.6$ and $86 \leq D \leq 100h_{50}^{-1}$ kpc.

The nearly edge-on spiral galaxy (object #5) is clearly visible, $3.86''$ south to the quasar sightline. Its color is $m_{702} - m_{814} = -0.1$, which indicates a flat spectrum. It is the most likely candidate for the $z_d = 0.7443$ absorber, with an impact parameter of $38h_{50}^{-1}$ kpc and an absolute magnitude $M_B = -22.9$. Assuming that this galaxy is strictly edge-on, then the absorbing clouds are located $9h_{50}^{-1}$ kpc above the galactic plane, at a projected distance of $36h_{50}^{-1}$ kpc from the galactic center.

4. Discussion

At $z \sim 2-3$, the 21cm/damped Ly α absorption-selected galaxies are assumed to trace protogalactic disks, as first proposed by Wolfe et al. (1986). The aim of our survey is to ascertain whether or not the HI cross-section selected objects belong to an homogeneous class of galaxies and to derive the main properties of the HI absorbers: size, absolute luminosity, morphology and color.

At the time of the target selection, there was no DLAS known at low redshift. Our sample includes systems with either 21 cm absorption and/or strong Fe II relative to Mg II absorption (Bergeron & Stasińska 1986). One of the strong Fe II absorbers has been confirmed to be a damped Ly α system, and the two others are candidate damped Ly α systems, with $5 < w_r < 10$ Å. The sample comprised seven candidates or confirmed DLAS at $0.4 \leq z \leq 1.0$ and a confirmed one at $z_d = 1.776$ towards seven quasars.

A first important result of our study is the presence of candidate absorbers in seven cases at projected distances $\theta < 1.6''$ from the quasar sightline with apparent magnitudes brighter than our 5σ threshold $m_{702, \text{lim}} \simeq 25.9$. The last case, with $\theta = 3.86''$, is a spiral galaxy with a favorable edge-on geometry. The rest-frame B magnitudes of the damped Ly α candidate absorbers cover the range $-23.0 \leq M_B \leq -18.9$. The physical parameters of the candidate absorbers are listed in Table 9.

A most striking result is the wide variety of morphological types together with a large spread in luminosity: the damped Ly α absorbers do not constitute an homogeneous class of galaxies. Even if for a few fields, the identification of the absorber requires spectroscopic confirmation (existence of more than one possible candidates), there are unambiguous cases of very compact candidate absorbers. A prime example is object #2 in the field of PKS 0454+039: aside from a dwarf galaxy at low redshift (object #3 at $z = 0.072$), there is no other object detected within $5''$ from the quasar image. This candidate is barely resolved and after PSF subtraction, we get a FWHM for its core of $1.1h_{50}^{-1}$ kpc, with a possible underlying diffuse envelope

of $3.8h_{50}^{-1}$ kpc in linear extent. The sample also comprises spiral galaxies of normal linear sizes, as those detected in the fields of Q 1209+107 and MC 1331+170, and one of extremely large extent ($\sim 70h_{50}^{-1}$ kpc) in the field of 3C 196. The latter two are fairly bright with k -corrected (Sbc type) luminosities of $L_B \simeq 5.7$ and $2.7L_B^*$. There are two case of amorphous morphology, one of fairly high surface brightness (object #3 in the field of PKS 1229–021), and the other one, towards 3C 286, has a moderately bright core surrounded by a very low surface brightness envelope detected only on a ground-based I -band image (Steidel et al. 1994a). The central part of this galaxy has a luminosity of the order of L^* if at $z_d = 0.692$. In several of the above cases, high HI column density gas is thus present in regions of low stellar density.

These results show that the damped Ly α population strongly differ from the Mg II absorption-selected galaxies, the latter being a well defined class of objects with homogeneous properties (BB91, Bergeron et al. 1992, Steidel 1993, Steidel et al. 1994b, GB). The Mg II absorbers have blue B–K colors and show signs of recent stellar formation activity. They are fairly luminous, $-24.0 \leq M_{AB}(B) \leq -19.4$, field galaxies with only one known case of a dwarf galaxy at low z (< 0.1) with $M_{AB}(B) = -17.2$, although LMC-type Mg II absorption-selected galaxies could have been identified up to at least $z \sim 0.3$ (Le Brun et al. 1993, GB). These galaxies are characterized by large gaseous halos of typical size $D = 75(L/L_*)^{0.3}h_{50}^{-1}$ kpc and abundances $[Z/H] \sim -0.1$ to -0.3 at $z \sim 0.5$ (Bergeron et al. 1994).

In three cases, we find an excess of galaxies in the quasar field. Towards 3C 196 and PKS 1229–021, the quasar redshift is moderate ($z_e = 0.871$ and 1.038) and the detected galaxy excess could trace a group to which the radio-loud quasar belongs. Quasar host galaxies of high luminosity have also been tentatively detected for 3C 196 and 3C 286.

In our study, we find several cases of galaxies very close on the sky to background quasars and with redshifts of about 0.5 (if these galaxies are assumed to be the damped Ly α absorbers). This is an ideal situation in which multiple images of the quasar induced by gravitational deflection may be expected. Further, since we have deep and high-spatial resolution frames, secondary images of the QSOs induced by the absorber could be found easily, even if the angular separation to the primary image and the image flux ratio are small. However, in none of the investigated fields do we find any evidence for multiple images. In some cases, a faint secondary image may be difficult to find if it appeared superimposed onto the image of the intervening galaxy (3C 196, 3C 286). For PKS 1229–021, object #2 could have been a secondary image but, it is much more likely to be intrinsic emission from the jet, as indicated by the remarkable coincidence between the optical and radio knots (see Sect. 3.5). Around PKS 0454+039 and Q 1209+107 for instance, we estimate that we can

Table 9. Characteristics of the damped Ly α absorber candidates and of the other objects with smallest impact parameter

z_d or z_a^a	Obj.	D^b	M_B^c	size ^{b,d}	Comments	
0302–223 field : $z_e = 1.400$, $z_d = 1.0095$						
1.0095	2	12.0	–20.4	4.0×3.0	Semi compact	
	3	27.4	–22.0	1×2	Compact	
	7	84.3	–23.4	7.0×6.4	$z_g = 1.0095(1)$	
0454+039 field : $z_e = 1.345$, $z_d = 0.8596$						
0.8596	2	8.3	–20.5	1×1	Compact (2)	
0809+483 field : $z_e = 0.871$, $z_d = 0.437$						
0.437	4	12.5	–22.1	67×19	Giant Sbc (3)	
		(Bar)	–21.6			
0.871	2	<3.1	<–23.1	25×20	QSO host gal.	
	3	11.5	–22.0	20×10	QSO Comp.	
1209+107 field : $z_e = 2.191$, $z_d = 0.6295$						
0.6295	2	14.6	–22.0	17.1×7.1	Spiral Gal.	
1229–021 field : $z_e = 1.038$, $z_d = 0.39498$						
0.39498	3	9.9	–18.9	8.8×9.0	LSB	
	1.038	2	6.6	Unres.	Radio knot	
		4	15.5	–19.6	Unres.	Radio knot
		6	19.9	–18.7	Unres.	Radio knot
1328+307 field : $z_e = 0.849$, $z_d = 0.692$						
0.692	2c	8.5	–20.5	8.7×5.3	DLAS cand.	
	2a 2b	<2.8	<–22.3	27×11	QSO host gal.?	
1331+170 field : $z_e = 2.084$, $z_d = 0.7443, 1.776$						
0.7443	5	37.7	–22.9	22.5×3.9	Edge-on Spiral	
	1.776	2	9.5	–23.0 ^{e,f}	Unres.	
3		20.0	–22.7 ^e	Unres. $\times 1$	Compact	

^a The redshifts of the DLAS and DLAS candidates are written in bold characters

^b All impact parameters are given in unit of h_{50}^{-1} kpc

^c The absolute magnitudes have been calculated assuming $z_g = z_d$ (or z_a), with k -correction (see text for details)

^d For objects labeled as “compact”, the size is calculated from the deconvolved angular size of the object, $\sqrt{fwhm_{obj}^2 - fwhm_{psf}^2}$. For well resolved objects, the extent of the 1.5σ isophote is given

^e These magnitudes are derived from the F814W images

^f This magnitude may be strongly affected by the subtraction residuals

References : 1 - GB, 2 - Steidel et al. (1995), 3 - Cohen et al. (1996)

rule out the presence of an unresolved object at an angular distance exceeding $0.4''$ from the quasar and with a

flux ratio to the primary image greater than about 0.001. Among the confirmed gravitational lenses (see e.g. Refsdal & Surdej 1994), angular separations and flux ratio well above these limits have been observed. This already tells us that the mass of the dark halo in these lensing galaxies is much larger than that of the ordinary “absorption-selected” galaxies discussed in this study. Our negative result is also consistent with the fact that in gravitational lenses, several galaxies are often at work to produce the multiple images. We thus note that our data could be used to set tight constraints on the mass and/or mass distribution of the absorbing galaxies. This would require a detailed analysis of each individual case, which is beyond the scope of this study.

Acknowledgements. We are very grateful to Dr. P. Kronberg for providing us with its high resolution radio data of PKS 1229–021. We also would like to thank R. Hook (ST-ECF), P. Møller (STScI) and M. Giavalisco (STScI) for very useful advice concerning profile subtraction, and B. Fort and J. Roland for very helpful discussions about multiple gravitational images and optical emission associated with radio sources. We also thank the referee, M. Dickinson, for very useful remarks

References

- Arnaud J., Hammer F., Jones J., Le Fevre O., 1988, *A&A*, 206, L5
- Bergeron J., Boissé P., 1991, *A&A* 243, 344 (BB91)
- Bergeron J., Cristiani S., Shaver P., 1992, *A&A* 257, 417
- Bergeron J., Petitjean P., Sargent W.L.W., et al., 1994, *ApJ* 436, 33
- Bergeron J., Stasińska G., 1986, *A&A* 169, 1
- Bertin E., Arnouts S., 1996, *A&A*, in press
- Boissé P., Bergeron J., Le Brun V., Deharveng J.-M., 1996, in preparation
- Boissé P., Boulade O., 1990, *A&A*, 236, 291
- Briggs F.H., Turnshek D.A., Schaeffer J., Wolfe A.M., 1985, *ApJ* 293, 387
- Bridle A.M., Fomalont E.B., Patimaka J.J., Willis A.G., 1981, *ApJ* 248, 499
- Brown R.L., Mitchell K.J., 1983, *ApJ* 264, 87
- Brown R.L., Roberts M.S., 1973, *ApJ* 184, L7
- Brown R.L., Spencer R.E., 1979, *ApJ* 230, L1
- Brown R.L., Broderick J.J., Johnston K.J., 1988, *ApJ* 329, 138
- Carilli C.L., van Gorkom J.H., 1989, *Nature* 338, 134
- Chaffee F.H. Jr, Black J.H., Foltz C.B., 1988, *ApJ* 335, 584
- Coleman G.D., Wu C.-C., Weedman D.W., 1980, *ApJS* 43, 393
- Churchill C.W., Vogt S.S., Steidel C.C., 1995, From metal-line absorption profiles to halo kinematics. In: Meylan G. (ed.) *QSO absorption lines*, Springer, Berlin, p. 153
- Cohen R.D., Barlow T.A., Beaver E.A., et al., 1994, *ApJ* 421, 453
- Cohen R.D., Beaver E.A., Diplax A., et al., 1996, *ApJ* 456, 132
- Cristiani S., 1987, *A&A* 175, L1
- Dey A., van Breugel W.J.M., 1994, *AJ* 107, 1977
- Foltz C.B., Chaffee F.H., Wolfe A.M., 1988, *ApJ* 335, 35
- Frei Z., Gunn J.E., 1994, *AJ* 108, 1476
- Guillemain P., Bergeron J., 1996, *A&A*, submitted (GB)
- Holtzman J.A., Burrows C.J., Casertano S., et al., 1995, *PASP* 107, 1065
- Koratkar A.P., Kinney A. L., Bohlin R.C, 1992, *ApJ* 400, 435
- Kronberg P.P., Perry J.J., Zukowski E.L., 1992, *ApJ* 387, 528
- Lanzetta K.M., Bowen D.V., 1992, *ApJ* 391, 48
- Lanzetta K.M., Turnshek D.A., Sandoval J., 1992, *ApJS* 84,109
- Lanzetta K.M., Wolfe A.M., Turnshek D.A., 1995, *ApJ* 440, 435
- Le Brun V., Bergeron J., Boissé P., Christian C., 1993, *A&A* 279, 31
- Le Brun V., Bergeron J., Boissé P., 1997, in preparation
- Oren A.L., Wolfe A.M., 1995, *ApJ* 445, 6240
- Mc Gaugh S.S., 1994, *ApJ* 426, 135
- Miley G.K., Heckman T.M., Butcher H.R., van Breugel W.J.M., 1981, *ApJ* 247,L5
- Meyer D.M., York D.G., 1992, *ApJ* 399, L121
- Petitjean P., Bergeron J., 1990, *A&A* 231, 309
- Pettini M., Smith L.J., Hunstead R.W., King D.L., 1994, *ApJ* 426, 79
- Refsdal S., Surdej J., 1994, *Rep Prog Phys* 56, 117
- Sargent W.L.W., Boksenberg A., Steidel C.C., 1988, *ApJS* 68, 539
- Spencer R.E., Schilizzi R.T., Fanti C., et al., 1991, *MNRAS* 250, 225
- Spinrad H., McKee C., 1979, *ApJ* 232, 54
- Steidel C.C., 1993, The properties of absorption line selected high redshift galaxies. In Schull J.M., Thronson H. (eds.) *The evolution of galaxies and their environment*, Proceedings of the Third Grand Teton Summer Astrophysics Conference, Kluwer, Dordrecht
- Steidel C.C., Dickinson M., Bowen D.V., 1993, *ApJ* 413, L77
- Steidel C.C., Pettini M., Dickinson M., Persson S.E., 1994a, *AJ* 108, 2046 (SPDP)
- Steidel C.C., Bowen D.V., Blades J.C., Dickinson M., 1995, *ApJ* 440, L45
- Steidel C.C., Dickinson M., Persson S.E., 1994b, *ApJ* 437, L75
- Steidel C.C., Sargent W.L.W., 1992, *ApJS* 80, 1
- van Breugel W.J.M., Fanti C., Fanti R., 1992, *A&A* 256, 56
- Whitmore B., 1995, Photometry with the WFPC2. In: Koratkar A., Leitherer C. (eds.) *Calibrating Hubble Space Telescope: Post servicing mission*, STScI, Baltimore
- Wolfe A.M., 1987, In: Blades J.C., Turnshek D.A., Norman C.A. (eds.) *QSO Absorption Lines: Probing the Universe*, Cambridge University Press, p.297
- Wolfe A.M., Davis M.M., 1979, *AJ* 84, 699
- Wolfe A.M., Turnshek D.A., Smith H.E., Cohen R.S., 1986, *ApJS* 61, 249
- Young P., Sargent W.L.W., Boksenberg A., 1982, *ApJS* 48, 455

This figure "q3c196field.jpg" is available in "jpg" format from:

<http://arxiv.org/ps/astro-ph/9611031v1>

This figure "q3c286field.jpg" is available in "jpg" format from:

<http://arxiv.org/ps/astro-ph/9611031v1>

This figure "ex0302field.jpg" is available in "jpg" format from:

<http://arxiv.org/ps/astro-ph/9611031v1>

This figure "q1209field.jpg" is available in "jpg" format from:

<http://arxiv.org/ps/astro-ph/9611031v1>

This figure "q1229field.jpg" is available in "jpg" format from:

<http://arxiv.org/ps/astro-ph/9611031v1>

This figure "mc1331field.jpg" is available in "jpg" format from:

<http://arxiv.org/ps/astro-ph/9611031v1>

This figure "q0454field.jpg" is available in "jpg" format from:

<http://arxiv.org/ps/astro-ph/9611031v1>